

**Antarctic coastal polynyas  
as observed with passive satellite sensors:  
Total area, ice production, brine release,  
and thin-ice thickness and area  
for the period 1992-2006**

ME 487/40-1 and 40-2, STA 410/6-3, and HE 1746/10-1 to 10-3

Final Report

Detlef Stammer, Jens Meincke  
Zentrum für Marine und Atmosphärische Wissenschaften  
Institut für Ozeanographie  
Universität Hamburg

Georg Heygster  
Institut für Umweltphysik  
Universität Bremen

April 2008

Executive Summary .....	3
Changes to the work plan .....	3
1. Acquire and project SSM/I and AMSR-E data (3.2.1) .....	4
1.1 SSM/I data acquisition .....	4
1.2 SSM/I data projection.....	5
1.3 AMSR-E data acquisition and geo-location.....	7
2 Set up of PSSM (3.2.2).....	8
2.1 Set up of PSSM for SSM/I data .....	8
2.2 Set up of PSSM for AMSR-E data.....	15
3 Set up of other software (3.2.3).....	16
4 Acquire and project evaluation and other data (3.2.4) .....	16
5 Apply & evaluate PSSM on test periods and regions (3.2.5).....	20
5.1. Evaluation of the PSSM based on SSM/I data .....	20
5.2 Validation of ASI/AMSR-E ice concentrations .....	23
6 Perform analysis of ice production (3.2.6).....	24
7 Comparison with models (3.2.7).....	26
7.1 Kara Sea .....	26
7.2. Southern Ocean .....	27
8 Get polynya area time-series (3.2.8) .....	31
8.1. Kara Sea polynya area.....	31
8.2 Polynya area: Central Weddell Sea (CWS).....	32
8.3 Polynya area: Eastern Weddell Sea (EWS).....	37
8.4 Polynya area: Western Indian Ocean Sector (WIS).....	41
8.5 Polynya area: Eastern Indian Ocean Sector (EIS).....	44
8.6 Polynya area: Western Pacific Ocean Sector (WPS) .....	47
8.7 Polynya area: Eastern Pacific Ocean Sector (EPS).....	51
8.8 Polynya area: Western Ross Sea (WRS).....	54
8.9 Polynya area: Western Bellingshausen Sea (WBS) .....	58
8.10 Polynya area: Eastern Bellingshausen Sea (EBS).....	63
8.11 Summary of PSSM areas.....	66
9 Get ice production, etc. time-series & comparison with models .....	69
9.1 Methodology .....	69
9.2 Ice and Salt Production CWS.....	70
9.3 Ice and Salt Production EWS .....	74
9.4 Ice and Salt Production WIS .....	76
9.5 Ice and Salt Production EIS .....	77
9.6 Ice and Salt Production WPS .....	81
9.7 Ice and Salt Production EPS.....	84
9.8 Ice and Salt Production WRS.....	88
9.9 Ice and Salt Production WBS.....	93
9.10 Ice and Salt Production EBS .....	95
9.11 Ice and Salt Production: Summary.....	96
10 Comparison of thin-ice thickness SSM/I vs. AMSR-E (3.2.10).....	99
10.1 Thin-ice thickness based on SSM/I data .....	99
10.2 Thin-ice thickness based on AMSR-E data.....	111
Summary of the Results .....	112
11 Acknowledgments .....	114
12 References .....	114
13 Conference contributions, Reports, Theses, and Manuscripts .....	117
14 Peer reviewed publications.....	118
15 Enclosed Articles and Manuscripts .....	119

## Executive Summary

The Polynya Signature Simulation Method (PSSM) allows to obtain polynya area and sea ice edge with an accuracy of about 200 km<sup>2</sup> and 10 km, respectively, using an iterative classification of data acquired by the satellite microwave radiometer Special Sensor Microwave/ Imager (SSM/I) into three different surface types: open water, thin ice, and thick ice. A modified version of the PSSM is used here to estimate the daily total area occupied by Antarctic coastal polynyas for the period 1992-2005 and polynyas in the Kara Sea, Arctic, for the period 1995-2004. The total area comprises the fraction of open water and thin ice up to a thickness of approximately ten centimeters. The most important modifications enclose generation and usage of a new, high-resolution Antarctic land mask, filtering of ambiguous polynya area retrievals caused by shelf ice / icebergs / fast ice, and utilization of regionally varying tie points as required by the classification. Satellite infrared and visible imagery are used in combination with meteorological data in order to estimate ice production, brine release and the thin-ice area and thickness for the polynya areas. Data from the new satellite microwave radiometer Advanced Microwave Scanning Radiometer (AMSR-E) aboard AQUA are used to obtain high-resolution ice concentration, which is combined with the results of the PSSM to enhance the robustness of the ice production estimates. The main results of this project, which have partly been already published or are going to be published soon in 5 papers (see Section 14) (at least three more papers are in preparation) are as follows:

- The average wintertime (June-Aug.) total circum-Antarctic polynya area amounts about (235 000 ± 12 400) km<sup>2</sup>; the largest contribution to this area is made by polynyas along East Antarctica and the Ross Sea.
- The most frequent polynyas are the Mertz Glacier polynya, the Cape Darnley polynya and the Terra Nova Bay polynya; these occurred on average on at least 80% of all days during winter.
- The average winter-time polynya area of Antarctic coastal polynyas seems to have been constant during 1992-2005 in almost all investigated regions.
- The average winter-time (Jan.-Apr.) Kara Sea polynya area is (25 030 ± 7 185) km<sup>2</sup> for the period 1995-2004; an extension of this time series to the period 1979-2004 reveals an increase in the total Kara Sea polynya area by 2400 km<sup>2</sup> / decade.
- The average wintertime (June-Aug.) total circum-Antarctic ice production is about 860 km<sup>3</sup> with an uncertainty of between 15 and 30 %; for the period May-Sep. this production is about 1600 km<sup>3</sup>. These two values translate into an average salt production of about 19 x 10<sup>12</sup> kg and 36 x 10<sup>12</sup> kg, respectively.
- Based on an under-estimation of the surface wind speed of up to 23 m/s (Mertz Glacier polynya) as derived from co-located automatic weather station data and ERA40 re-analysis data and the influence of this under-estimation on the heat flux calculation, it can be assumed that the ice production obtained in this study for polynyas that are situated in regions with a particularly steep topography could be twice as large as given here.

## Changes to the work plan

Project activities in Hamburg focused on a set of modifications of the PSSM, a better handling of ambiguous classification results, and the derivation of supervised, temporally consistent, quality checked time-series of the polynya area and the associated ice and salt production. These activities include in particular development, testing and application of special masking and filtering approaches to remove ambiguities in the ice type classification

done with the PSSM. Moreover, in order to minimize the effect of an old, static land-mask of Antarctica with just 25 km grid cell size, a new one has been developed, which is up-dated every other year in those regions of the Antarctic, which are subject to notable changes in the shelf ice border line, and which has 5 km grid cell size. These activities were partly carried out at the expense of other work that has been proposed: the Kara Sea polynya area time-series spans just years 1995-2004 and the Antarctic polynya area time series stops in 2005 instead of 2006.

The results obtained with regard to the polynya area did not suggest to emphasizing on a daily cycle of the polynya area. Instead, the computed ice production values have been checked extensively with those available from previous and recent studies, triggering a comparison between the used model data and independent in-situ data to judge the quality of the obtained results.

Regarding the retrieval of the thickness of thin ice the activities focused on the adaptation of a new algorithm based on SSM/I data, which was developed recently by others, to the Antarctic environmental conditions. This adaptation failed because of too variable sea-ice surface properties. Instead the method was exemplarily applied as it is in order to obtain information about the ice thickness that is typically found within the polynyas as identified with the modified PSSM. New results obtained from in-situ observations of thin ice by others suggest that this new method is in fact quite sensitive to the surface properties of thin ice and therefore has just been applied to the Ross Sea.

Project activities in Bremen focused on the ARTIST Sea Ice (ASI) algorithm, its application to data of the Advanced Microwave Scanning Radiometer (AMSR-E), and its validation under various conditions, especially thin ice. The reason is the good agreement in horizontal resolution of the PSSM/SSMI and ASI/AMSR-E data and results. The additional confidence obtained by validations of the ASI algorithm under various conditions serves for better results when developing combined applications as is done in this study.

The originally proposed resolution harmonization of the AMSR-E data using the Backus-Gilbert technique turned out to be much more time consuming than was originally thought, because of a so far undetected geo-location problem of the AMSR-E data. This problem has been solved now. However, this proposed resolution harmonization, the adaptation of the PSSM to AMSR-E data (Work Program, 3.2.2), and the application of the PSSM on AMSR-E data (3.2.5) with a subsequent generation of a polynya area time-series based on AMSR-E data (Work Program, 3.2.8) were not carried out within this project.

## 1. Acquire and project SSM/I and AMSR-E data (3.2.1)

### 1.1 SSM/I data acquisition

In principle, data of the Special Sensor Microwave/Imager (SSM/I) is available since June/July 1987. However, in order to use the Ice Edge Detection (IED) method and the Polynya Signature Simulation Method (PSSM), the 85.5 GHz channels of the SSM/I are required. These channels suffered from serious noise problems starting in 1988 and ending in 1991 and therefore cannot be used. Data acquisition therefore has to begin with data starting December 1991 acquired by SSM/I sensor aboard DMSP platforms f10 and f11. SSM/I data are available from aboard the following DMSP platforms for the given periods:

- f10: December 1990 to November 1997
- f11: December 1991 to November 2000
- f13: April 1995 until present
- f14: May 1997 until present
- f15: February 2000 until present

SSM/I data can be obtained from various sources and in various formats: as brightness temperatures already projected into a polar-stereographic grid (NSIDC-grid, EASE-grid), as orbital brightness temperatures (i.e. together with the latitude and longitude information of the center of each effective field-of-view, EFOV, on the ground), and as antenna temperatures. In order to obtain optimal spatial resolution and in order to apply the Backus-Gilbert interpolation technique as proposed, orbital data are required. Actual and more recent data have been downloaded automatically from <ftp://ghrc.msfc.nasa.gov>, starting with day 134 of year 2002 until present for DMSP-f13, -f14, and -f15. These are orbital brightness temperatures. Data from DMSP platform f16 are not yet available from this ftp-server. Data prior to this date are obtained in collaboration from the Max-Planck-Institute for Meteorology from the NOAA-NESDIS archive. Until present, the data download is as follows:

- f13 - f15: completed for the project but ongoing until today
- f10, f11: completed

## 1.2 SSM/I data projection

NOAA-NESDIS SSM/I data is antenna temperatures, which need to be converted into brightness temperatures first. This has been done using software (FORTRAN, C++) provided by NOAA NESDIS. This software has been embedded into an IDL-routine, which allows to converting large amounts of antenna temperatures into brightness temperatures and a consistency check by plotting the brightness temperatures channel by channel.

The next step for both MSFC and NOAA data is to interpolate and project it into the NSIDC polar-stereographic grid (NSIDC, 1996). The interpolation is done using the Backus-Gilbert-Interpolation technique, which permits some resolution improvement (Stogryn, 1978; Hunewinkel et al., 1998), and the drop-into-the-bucket method together with the latitude/longitude information provided with the SSM/I data. The 37 GHz data is projected into the 12.5 km x 12.5 km NSIDC grid (is used for the 85 GHz data originally); 85 GHz data is projected into a fine-mesh version of this grid with 5 km x 5 km grid-cell size. Prior to the interpolation an algorithm seeks for missing scan lines and scan lines, which are not located correctly. Where necessary, data of these scan lines is removed. The possible ambiguity between 0 and 360 degrees longitude when interpolating the data has been considered.

The conversion into brightness temperatures (NOAA-NESDIS data) and the interpolation and projection into the NSIDC polar-stereographic grid (NSIDC, 1996) has been completed. Data of the following periods has been processed:

- f15: Feb. 2000 – Oct. 2005 (but ongoing until today, i.e. Mar. 2008)
- f14: May 1997 – October 2005
- f13: May. 1995 – October 2005 (but ongoing until today, i.e. Mar. 2008)
- f11: Jan. 1997 – Nov. 2000 (Arctic)
- f10: Jan. 1995 – Nov. 1997 (Arctic)
- f10: Jan. 1992 – Nov. 1997 (Antarctic)

Data download and processing has been continued until today in a way, that enables to routinely get the most recent available data needed for the generation of polynya maps, which are subsequently put on the webpage of the IfM with a one day time lag to the acquisition by the SSM/I sensor.

At the end SSM/I data of DMSP platform f10, f13, and f15 is used. In order to obtain a homogeneous time series an inter-sensor calibration is required (e.g. Colton and Poe, 1999). For this purpose three different regions of the central high Antarctic continent each of size 90 000 km<sup>2</sup> have been selected. SSM/I data obtained at 37 GHz and 85 GHz, both polarizations, during June and July 1996 over these regions from aboard DMSP platform f10 and f13 and

during June and July 2002 from aboard DMSP platform f13 and f15 are compared with each other. Data of different platforms has to be acquired within a time difference of one hour to each other to be included in the comparison. The results of a linear regression between the data of two platforms is used to transform SSM/I data acquired from aboard the older platform onto the level of the newer platform, so that DMSP-f10 and DMSP-13 SSM/I data are converted onto the level of DMSP-f15 SSM/I data. Figure 1 shows, as a sample set the scatterplots of SSM/I brightness temperatures at 37 and 85 GHz as acquired by DMSP platform f13 and f15 in July 2002 over the three regions. Table 1 gives the respective conversion coefficients (bias and slope obtained with the linear regression) together with the mean RMS error and the mean linear correlation coefficient.

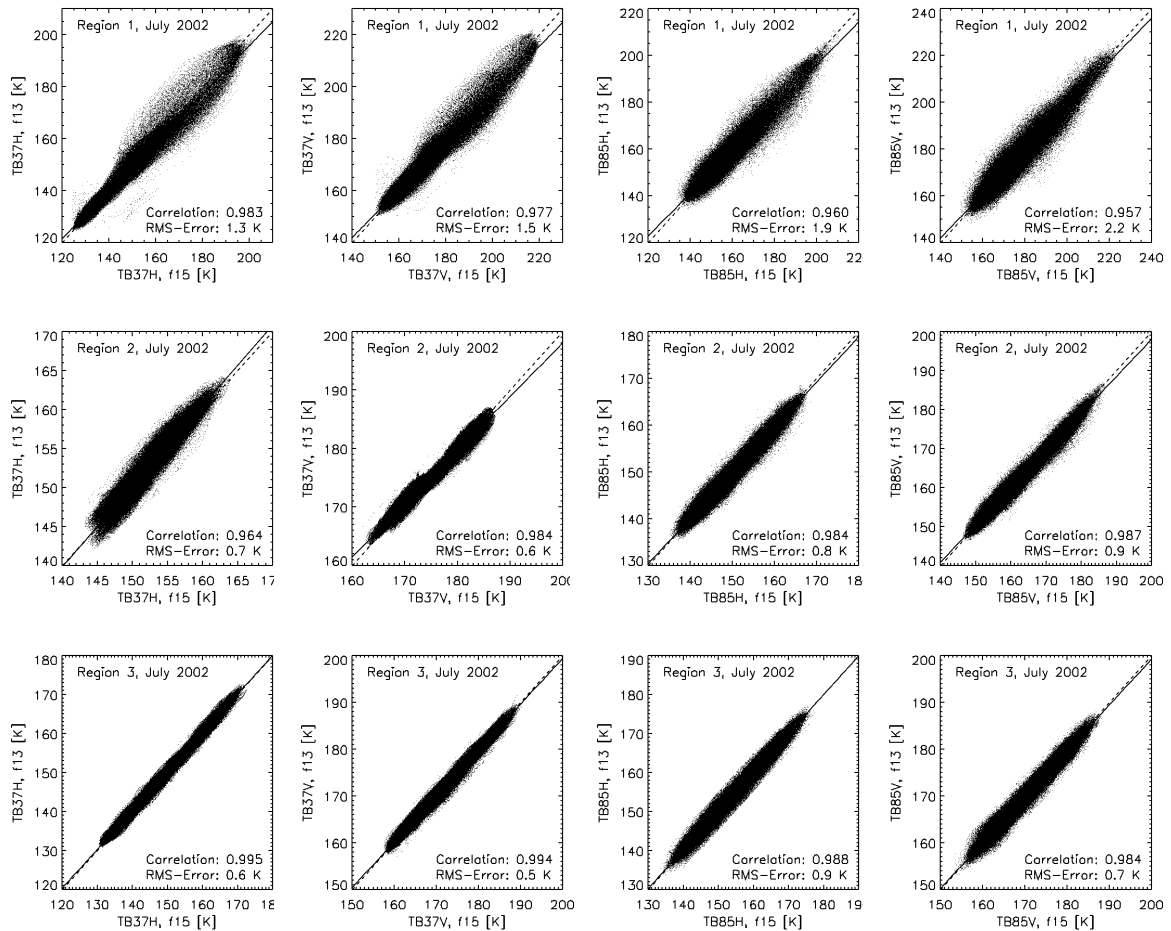


**Figure 1:** DMSP-f13 versus DMSP-f15 SSM/I brightness temperatures at 37 and 85 GHz as obtained over three different specifically selected regions of the high Antarctic continent within one hour time difference in July 2002. The letter H and V denotes horizontal and vertical polarization, respectively. The solid (dotted) line marks the line of perfect agreement (the linear regression line).

Coefficients for	37 GHz, h-pol.	37 GHz, v-pol.	85 GHz, h-pol.	85 GHz, v-pol.
F10 to F13: Bias	5.616585	1.943709	1.112833	5.033638
Slope	0.969523	0.991117	0.995633	0.971935
RMS	0.98 K	0.94 K	1.07 K	1.07 K
Correlation	0.969	0.928	0.968	0.971
F13 to F15: Bias	0.721235	-1.061621	2.727245	2.497620
Slope	0.993213	1.005835	0.981042	0.985856
RMS	0.85 K	0.85 K	1.03 K	1.20 K
Correlation	0.967	0.963	0.977	0.977

**Table 1:** Results of the linear regression of DMSP-f10 and -f13 and DMSP-f13 and -f15 37 and 85 GHz brightness temperatures obtained over three specifically selected regions in the high Antarctic continent during June/July 1996 and June/July 2002 (see Figure 1 and text).

### 1.3 AMSR-E data acquisition and geo-location

The complete AMSR-E L1A/B data are being collected at the University of Bremen (UB), together with the resulting ARTIST sea ice (ASI) algorithm concentrations (Kaleschke et al., 2001; Spreen et al., 2008). The complete archive is accessible for the public at [www.iup.uni-bremen.de/seaice/amsr](http://www.iup.uni-bremen.de/seaice/amsr). The originally planned resolution harmonized brightness temperature data set using the Backus-Gilbert interpolation method has not been established because of the geo-location problems of AMSR-E (see above). However, the geo-location problem has been solved, and the results have been published in Wiebe et al. (2008). The Backus-Gilbert interpolation is still in work.

The originally planned resolution harmonization of the different AMSR-E channels and frequencies required an exact geo-location, i.e. determination of the geographic latitude and longitude of the centre point of the footprint of the different channels. However, it has turned out the currently available Level 1a and Level 1 b AMSR-E data have an insufficient geo-location with errors of up to five kilometres. Therefore, as an initial step a geo-location correction had to be developed. This has been done in the master thesis of Wiebe (2007). The results are being published in Wiebe et al. (2008).

The process of determining the geographic latitude and longitude (short: lat/lon) of the centre point of the footprint is called geo-location, which is currently suboptimal for AMSR-E (Advanced Microwave Scanning Radiometer for Earth Observing System) Level 1 data provided by the Japan Aerospace Exploration Agency (JAXA). Here we present a study for improving the geo-location. The viewing angles (nadir angle and scan angle) that define the bore-sight direction of the instrument are optimized and new lat/lon coordinates are calculated. The optimization method is based on minimizing differences between ascending and descending swaths. The results of the here calculated viewing angles have an overall standard deviation of  $0.005^\circ$ , which is 170 m on ground for the nadir angle and 70 m for the scan angle. The residual geo-location error ranges between 425 m (89 GHz) and 1425 m (6 GHz). The averaged repositioning between JAXA and our geo-location ranges between 3.5 km and 7 km, i.e. in the order of one footprint size at 89 GHz. A comparison with a similar study performed by Wentz, shows good agreement in the viewing angles. The RMS of the differences is  $0.0083^\circ$  ( $\approx 283$  m) for the nadir angle and  $0.0132^\circ$  ( $\approx 191$  m) for the scan angle. As the geo-location problem has been solved only recently, the Backus-Gilbert interpolation of AMSR-E data is still in work.

## 2 Set up of PSSM (3.2.2)

### 2.1 Set up of PSSM for SSM/I data

The PSSM as developed by Markus and Burns (1995) and modified by Hunewinkel et al. (1998) has been further modified in order to cover two main issues of this project. First, this project aims at retrieving the open water as well as the thin-ice area of the polynya. It can be anticipated that in the polynya during cold conditions new ice forms and either covers the entire polynya or is advected towards the lee-side of the polynya. It is important to monitor this area in addition to the open water area. Furthermore, the open water area inside a polynya may be too small to be detected by the PSSM as such. But most likely the PSSM will be able to detect it as area of thin ice because a small open water area inside the SSM/Is' EFOV alters the measured brightness temperatures sufficiently towards a brightness temperatures being typical for thin ice. Hunewinkel et al. (1998) showed already some promising results for including thin ice into the IED and the PSSM. Second, this project aims at generating a time series of open water and thin ice extent for the period 1992-2006 for the entire Southern Ocean. Both require that tie points chosen for the analysis have to be valid for a) several months and b) for areas with different typical sea-ice types and therefore brightness temperatures.

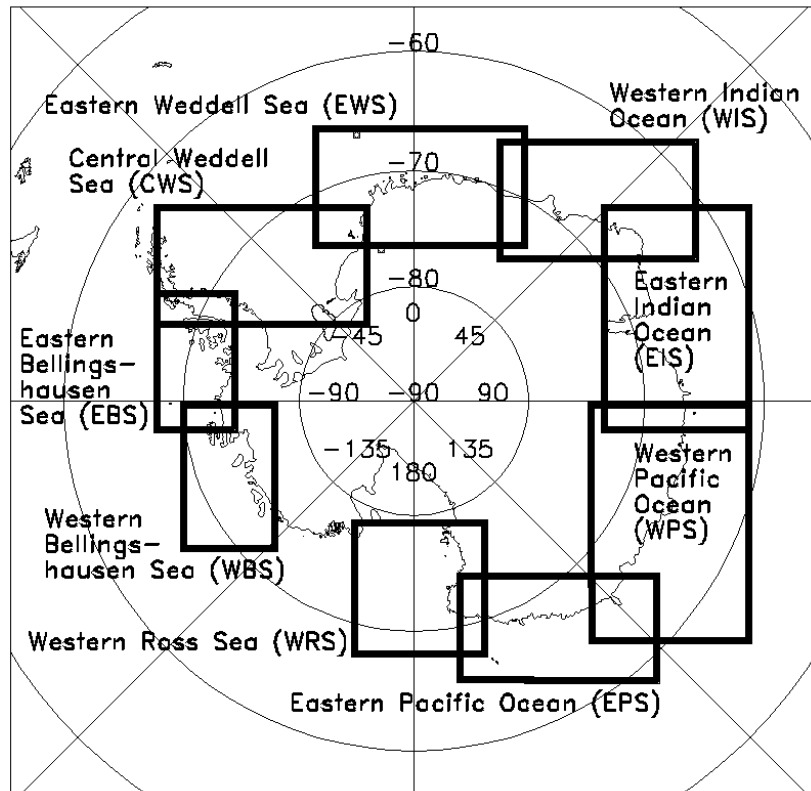
The PSSM used in this project is a combination of the IED and PSSM and works as follows (compare Markus and Burns, 1995; Hunewinkel et al., 1998):

- a) Calculate the brightness temperature polarization difference  $P$  for 37 GHz (12.5 km x 12.5 km grid-cell size) and 85 GHz (5 km x 5 km grid-cell size).
- b) Classify the map of  $P$  at 85 GHz into thick and/or consolidated ice and thin and/or loose ice plus open water using a threshold (tie point) separating typical values of  $P$  at 85 GHz for these surface types. This threshold is chosen somewhat arbitrarily at the beginning but is changed through the analysis (see below). The result is a 2-class binary map.
- c) To all grid cells of this binary map, which belong to the thick and/or consolidated ice class, the typical value of the  $P$  at 37 GHz (tie point) for this ice class is assigned. Because the thick and/or consolidated ice can be multiyear ice or first-year ice or exhibit surface/snow properties, which cause abnormal values for  $P$  at 37GHz, this tie point is calculated for every PSSM run. Only values of  $P$  at 37 GHz are used which belong to an area with more than 90 % ice concentration as calculated with the COMISO-Bootstrap algorithm (Comiso, 1995). Depending on region and season, this tie point takes values between 0.02 and 0.04. To all grid cells, which belong to the thin and/or loose ice plus open water class, the tie point at 37 GHz, which applies for this surface type is assigned. Here a fixed but region-dependent value between 0.08 and 0.09 is taken, which results from comparison of SSM/I data with AVHRR infrared data of polynyas with such an ice-water mixture. The result is called synthetic map of  $P$  at 37 GHz.
- d) This synthetic map is now convoluted with the antenna pattern of the 37 GHz channel of the SSM/I. The result is called simulated map of  $P$  at 37 GHz and contains high-resolution information about the above-mentioned surface types as would be viewed by the 37 GHz channels of the SSM/I.
- e) Measured and simulated map of  $P$  at 37 GHz are compared with each other by calculating the root-mean-square (RMS) difference and the correlation coefficient. The aim is by changing the tie point used in step 2) to iteratively optimize the result of this comparison, i.e., maximize the correlation and minimize the RMS difference. This iteration is done in the following way: First, the tie point is chosen to overestimate the thin and/or loose ice plus open water extent, i.e. it is close to the typical value for open water (0.2). The tie point is then reduced successively by a constant, loop-number

dependent (see below) increment (usually dividing between 0.2 and 0.02, the typical value for consolidated and/or thick ice), and for every new tie point synthetic and simulated maps of  $P$  at 37 GHz as well as correlation and RMS difference are calculated. The tie point with the best result gives the starting value for the next iteration loop and so on. On average about eight iteration loops are necessary to achieve stability in the resulting values of correlation and RMS difference (see Hunewinkel et al., 1998). The synthetic map belonging to the highest correlation/lowest RMS difference shows the most likely distribution of surface classes thick/consolidated ice and thin/loose ice plus open water.

- f) Repeat steps 2) to 5) considering only the thin/loose ice area plus open water, using a different start value for the tie point of  $P$  at 85 GHz, and using a fixed but region-dependent value between 0.170 and 0.182 as open water tie point for  $P$  at 37 GHz in order to detect any open water within the thin/loose ice area.

The introduced changes allow to applying the PSSM to estimate the open water and thin and/or loose ice area within a polynya. Moreover, the introduction of a variable thick and/or consolidated tie point allows to using the PSSM with the same configuration in a) different regions and b) for different typical thick and/or consolidated surface conditions.



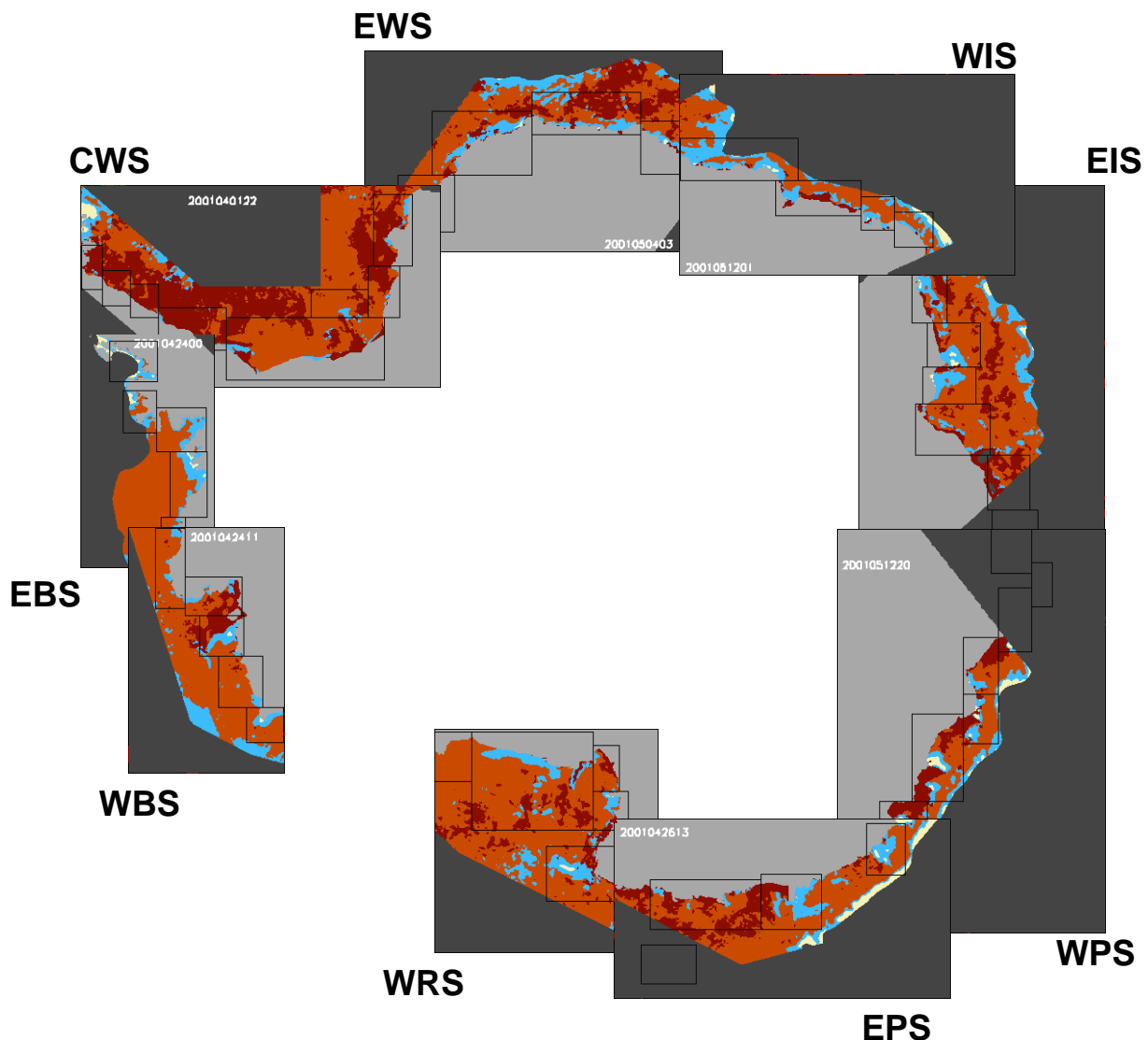
**Figure 2:** *Regions selected to apply the PSSM in the Southern Ocean.*

Figure 2 shows the nine regions, which are selected to apply the PSSM; these are (listed clockwise, starting at the Antarctic Peninsula, together with the most well-known polynyas within these regions):

- |                              |   |
|------------------------------|---|
| Central Weddell Sea          | (CWS), Ronne-Filchner Ice Shelf Polynya |
| Eastern Weddell Sea          | (EWS)                                   |
| Western Indian Ocean Sector  | (WIS)                                   |
| Eastern Indian Ocean Sector  | (EIS)                                   |
| Western Pacific Ocean Sector | (WPS)                                   |

Eastern Pacific Ocean Sector (EPS), Mertz Glacier Polynya  
 Western Ross Sea (WRS), Ross Ice Shelf and Terra Nova Bay polynyas  
 Western Bellingshausen Sea (WBS)  
 Eastern Bellingshausen Sea (EBS)

Not considered in this analysis is the northernmost part of the Antarctic Peninsula and the coast between the Ross Ice Shelf (Cape Colbeck) and Mount Siple (the gap between regions WRS and WBS). The latter area has been discarded because first analysis showed that a) there occur hardly any polynyas that are large enough to be identified with the PSSM, and b) the weather influence in this area often causes misclassifications. The northern Antarctic Peninsula has been discarded because of strong weather influences, and because of a short freezing season in this part of the Antarctic.



**Figure 3:** Sample PSSM maps of the polynya distribution around Antarctica. Open water, thin and/or loose ice, thick ice, and “stable ice” (see text) are given in pale yellow, blue, orange, and brown, respectively (see also Figure 4). The continent is flagged light grey. Missing data (caused by the finite swath width of the SSM/I), and masks to focus on polynya infested waters around the coast and to get rid of the influence of the open water regions beyond the ice edge (see text) are flagged dark grey. Black boxes within each region denote sub areas, which are explained and shown in more detail later.

A number of improvements and modifications turned out to be necessary after having applied the PSSM to a larger amount of data for the Southern Ocean. At first, cases where the brightness temperature polarization difference at 85 GHz for thick and/or consolidated ice exceeds a global threshold value of 0.035 were discarded from further analysis (Figure 4 f could be taken as an example of the effect that would be caused by NOT using such a threshold). It turned out that such high polarization differences are quite abundant over the Southern Ocean sea ice due to the weather influence on the sea-ice and snow properties. We used the polarization difference at 85 GHz instead of the one at 37 GHz (where this influence was observed to be stronger) because it allows to get rid of such cases with less ambiguity.

Secondly, two additional masks are applied. Both force the PSSM to focus on polynya infested waters around the coast. This was considered necessary because the polynya area tends to be underestimated when the marginal ice zone and the open water beyond the ice edge dominates the scene, i.e. a large portion of the polarization ratio shows the high values typical of open water. In this case the PSSM focuses on the large change in the polarization difference across the ice edge rather than on the smaller changes in the polarization difference associated with a polynya. The first mask simply flags the northern parts in each region. Figure 2 shows arbitrarily selected sample maps of the polynya distribution around Antarctica as obtained with the PSSM; the map of region CWS gives an example of this first mask. The second mask is generated from the biweekly average Comiso-Bootstrap algorithm sea ice concentration distribution. That region where this distribution takes values below 30% is considered as open water and accordingly is also discarded from further analysis. This mask is generated daily and relies on the ice concentrations of the two weeks before the day of interest. All regions except CWS, WRS, and WBS shown in Figure 3 give an example of this second mask. Depending on the ice concentration variability during the two weeks before the day of interest and this day itself, this second mask might not be able to completely mask out the open water area – particularly in case of a compact ice edge (see regions WIS, WPS, and EPS in Figure 3).

Thirdly, fast ice attached to the land or ice shelves often has a polarization difference, which is significantly above that of first-year ice. The same is valid for ice shelves and tabular icebergs. Consequently, the PSSM often misclassifies fast ice, ice shelves, and icebergs as thin and/or loose ice. For this reason it was necessary to develop a fast ice map. This turned out to be quite difficult because the polarization difference observed for Southern Ocean fast ice is quite variable, can be substantially influenced by weather effects, and exhibits a similar polarization difference as thin ice at all SSM/I frequencies. A first version of a fast ice map based on a region-dependent combination of different brightness temperature gradient ratios and the local polarization difference turned out to be insufficient. The used fast ice map, which is called “stable ice mask” henceforth, is based on the idea, that the polarization difference measured over a polynya should vary much more in time than the one obtained over an ice shelf, fast ice or a tabular iceberg. For this mask, the 85 GHz polarization ratio is temporally averaged over two weeks right before the day of interest for each grid cell. A threshold is applied to the resulting map, which selects areas with an average 85 GHz polarization ratio that is higher than that of first-year ice. The threshold is selected such that the selected area contains fast ice, shelf ice, icebergs and the polynya area (i.e. thin ice and/or open water). In order to separate the polynya area from the other types mentioned, this map is combined with the map of the temporal variability over the same period. By assuming that on a scale of two weeks the 85 GHz polarization ratio has a larger temporal variability over a polynya compared to fast ice/shelf ice/icebergs, the latter three types can be separated and assigned to the stable ice (SI) mask. This mask is subsequently applied to all PSSM maps.

Figure 4 demonstrates how this method works for the region WRS; it shows from left to right the biweekly average 85 GHz polarization ratio a), its corresponding temporal variability b), the actual 85 GHz polarization ratio c), the unfiltered PSSM polynya map d), and the filtered PSSM polynya map e). Image f) of this figure shows an example of the thin ice distribution as obtained with the method of Oshima et al. (2005). They use simple thresholds to estimate the areas covered by thick ice and thin ice of different thickness (0-10cm and 10-20 cm).

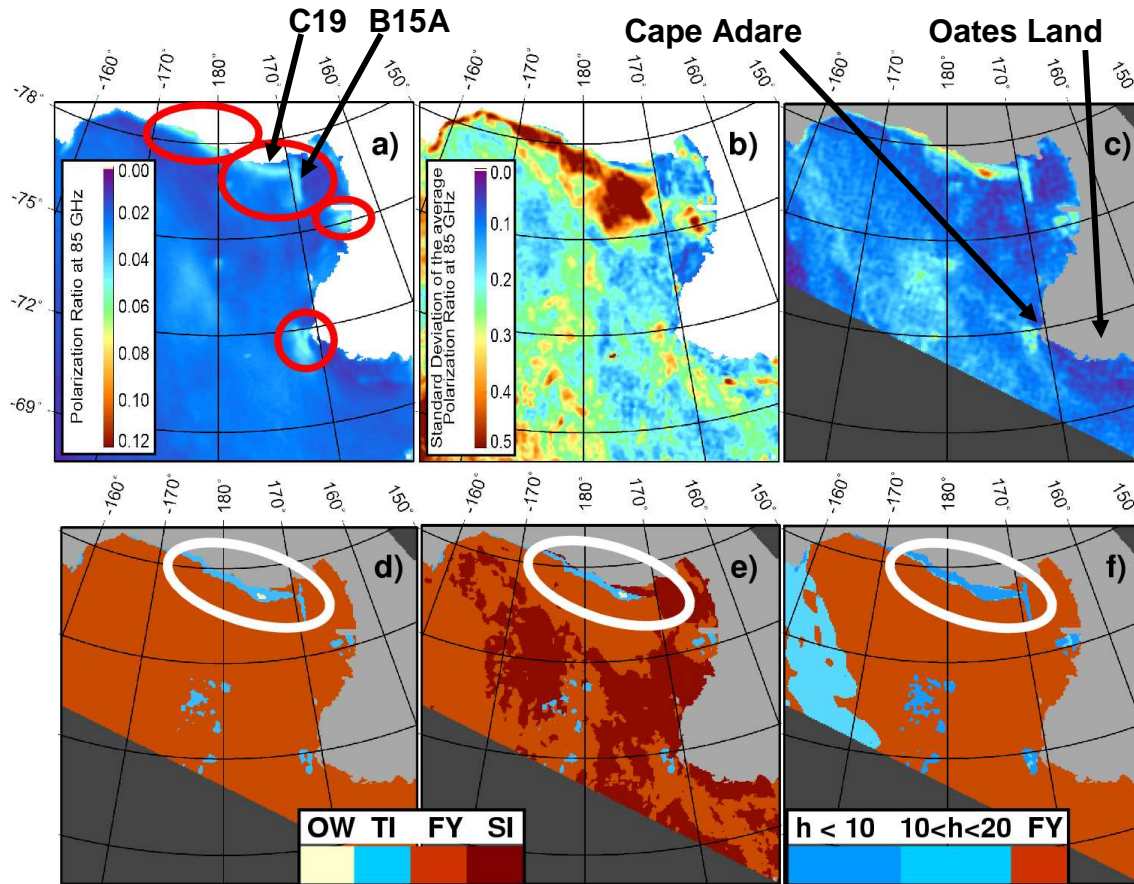


**Figure 4:** (a) Average 85 GHz polarization ratio (2 weeks) for region WRS; b) its variability; c) the actual 85 GHz polarization ratio (June 7 2002, 12 UTC); d) the resulting PSSM map; e) the same map after applying the mentioned mask (see text); f) polynya distribution after the method of Oshima et al. (2005) with  $h$  the ice thickness in centimeters. Polynyas and icebergs encircled red in a) exhibit elevated values of the 85 GHz polarization ratio. White ellipses in d)-f) mark the region where application of the stable ice (SI) mask mitigates misclassification of icebergs and fast ice as thin ice by the PSSM. Acronyms OW, TI, FY, and SI in the legend of d) and e) denote open water, thin ice, thick ice, and stable ice, respectively.

The red ellipses in image a) highlight areas containing elevated values of the biweekly average 85 GHz polarization ratio. These elevated values can be caused either by polynyas or by fast ice/shelf ice/tabular icebergs. In particular, the area of elevated 85 GHz polarization ratios, which extends along 170°E in the southwestern Ross Sea is caused by the giant tabular iceberg B15A (see e.g. Martin et al., 2007). Perpendicular to this one, a second giant tabular iceberg (C19) extends in east-west direction along the ice shelf border. These two areas exhibit a rather low temporal variability of the 85 GHz polarization ratio (Image b), while to the East and North of tabular iceberg C19 this variability is large. Applying the PSSM to the actual 85 GHz polarization ratio shown in image c) yields the polynya distribution map shown in image d). Areas occupied by the two mentioned tabular icebergs are misclassified as thin ice. Now, the map generated from the information given in images a) and b) reveals the stable

ice mask, which when applied to image d) yields image e). The misclassified areas are successfully flagged, while the polynyas along the Ross Ice Shelf, iceberg C19, the Terra Nova Bay, and at Cape Adare are preserved. Note that the stable ice mask flags also sea ice areas, which exhibited temporally stable conditions. In particular, the fast ice extending from Cape Adare westward along Oates Land is successfully marked as stable ice (image e).

Note also, that the simple method of Ohshima et al. (2005), which is based on threshold values of 0.045 and 0.056 applied to the 85 GHz and 37 GHz polarization ratio, respectively, does reveal a polynya distribution similar to the one obtained with the PSSM, except that a) fast ice/shelf ice/tabular icebergs need to be flagged as well, and b) the usage of the 37 GHz polarization ratio enhances the likelihood of misclassifications of areas where this ratio is potentially influenced by weather induced surface and sub-surface property variations.

However, the fast ice mask as described above tends to fail for very persistent polynyas, i.e. polynyas lasting longer than two weeks, because in this case the temporal variability of the 85 GHz polarization ratio falls below the threshold chosen to separate the polynya area from the regions occupied by fast ice/shelf ice/tabular icebergs. In order to get rid of this problem a post-processing step has been introduced. PSSM maps of one region of one month, which have already been filtered using the stable ice mask are read and manually checked for the occurrence of stable ice in an area, which should be occupied by a polynya. Subsequently, a revised stable ice mask is generated from the maximum number of consecutive PSSM maps of one month (at least of five days). This revised stable ice mask is then applied to all PSSM maps of that region of the particular month to obtain a revised, supervised set of filtered PSSM polynya distribution maps.

Forth, after having applied the PSSM to a larger amount of data for the Southern Ocean of the more recent years, it was decided to improve the land mask. The land mask being in use for SSM/I data is quite old and does not include changes in the extent of the Antarctic shelf ice, which took place over the last 15 years. It is essential for the estimation of the area covered by coastal polynyas, however, that the coastline is located as accurate as possible. For this purpose, the land mask was improved manually by using AVHRR clear-sky imagery, processed, calibrated and projected onto the NSIDC grid with 1km x 1km spatial resolution for each region given in Figure 2. Figure 5 shows the results of this very time consuming improvement of the land mask (about four weeks for one year) for 2002. Figure 6 gives a closer view of the achieved improvement for regions CWS, EPS and WRS. Because of the required effort, the fact that largest changes in the land mask can be expected for those regions (see Figure 1), which contain large and dynamic ice shelves, and the possibility to flag ice shelves in the final product using the stable ice mask described above, the improvement of the land mask has been carried once (2002) for the entire Antarctic, and for 1992, 1994, 1996, 1998, 2000, and 2002 for regions CWS, EIS, EPS, and WRS. Note that as a side effect of this work, the spatial resolution of the land mask is improved from 12.5 km to 5 km.

Finally, we have included the output of sort of a quality measure of the obtained PSSM polynya maps by storing the final polarization difference values, which mark the transition open water – thin ice and thin ice – thick ice for every overpass, and by calculating the daily mean value and its standard deviation of this final polarization difference. These values are subsequently used to rank the obtained PSSM polynya maps. If the final polarization difference value falls within the ranges given by the mean values (both transitions) plus or minus on standard deviation, then the polynya map is rated a good one. If both ranges are not met, the polynya map is considered a bad one – depending however, how large the ranges are. This turned out to be necessary to optimize the supervised selection of polynya maps used to generate time series of the polynya area (section 8).

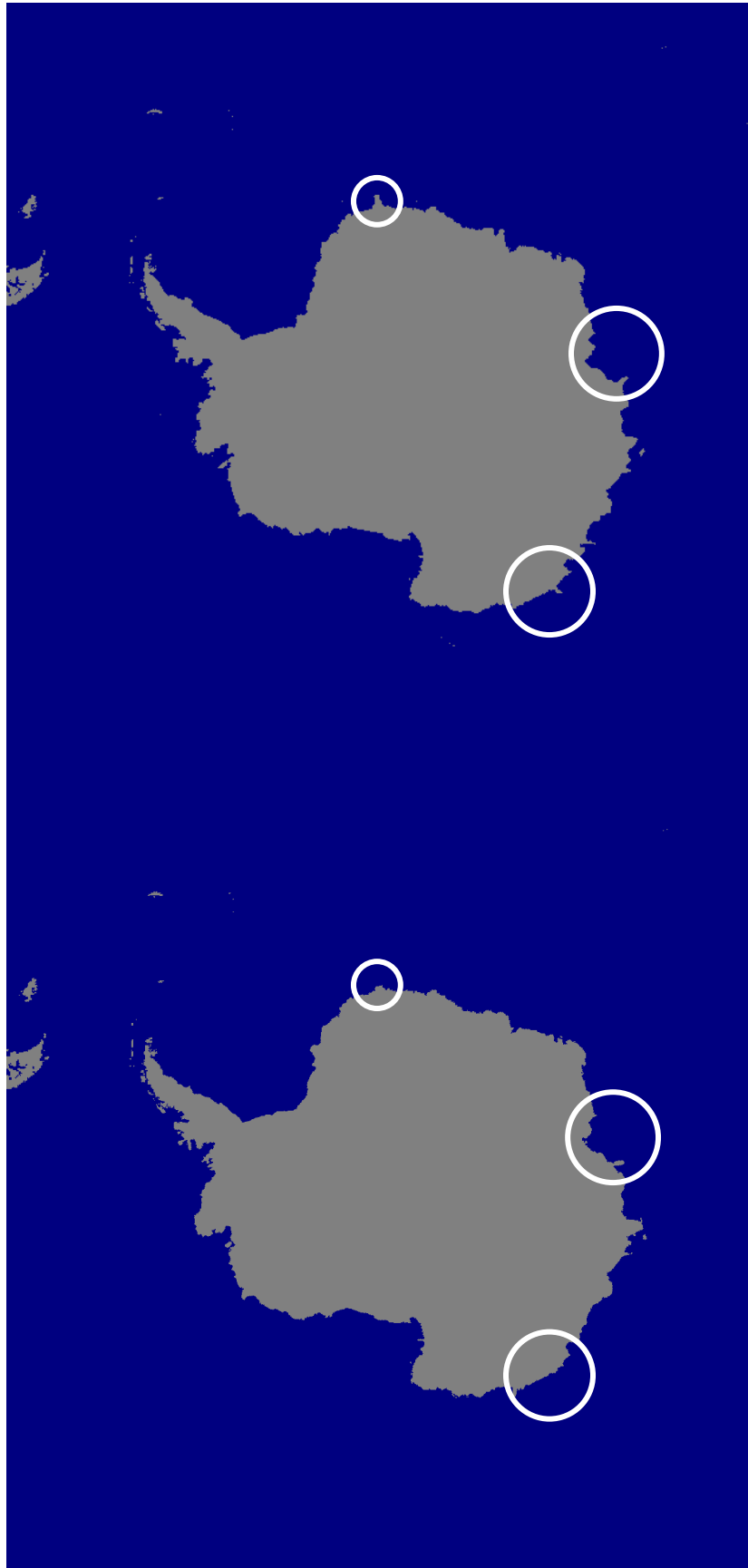


**Figure 5:** Antarctic land mask (*top = old, bottom = new, i.e. spring 2002*); some of the most obvious changes are marked by circles (see also Figure 6).

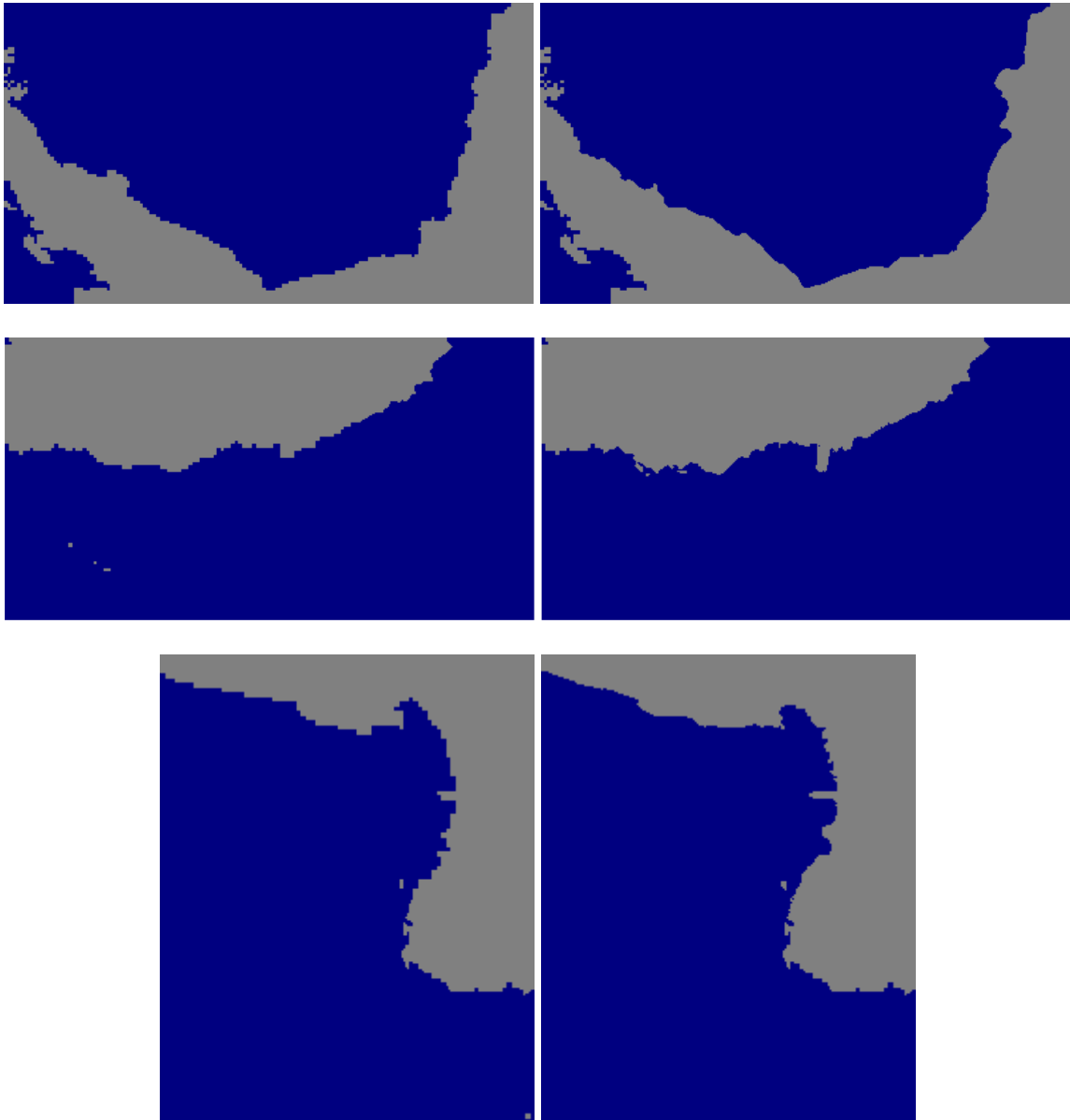


**Figure 6:** Antarctic land mask for selected regions (Top: CWS, Middle: EPS, Bottom: WRS, see also Figure 1), left = old, bottom = new, i.e. spring 2002.

## 2.2 Set up of PSSM for AMSR-E data

Because of the geo-location problem of the AMSR-E data, which has been solved within this study (Wiebe, 2007), the Backus-Gilbert interpolation of the AMSR-E data is a still ongoing work. Since this interpolation is regarded as important pre-requisite for the adaptation of the PSSM for its use with AMSR-E data, this method could not be adapted and not be applied to AMSR-E data. Accordingly, neither the circum-Antarctic polynya distribution as based on the PSSM applied to AMSR-E data (point 3.2.5 of the work plan for UB), nor a time series of such a distribution based on this data has been obtained (point 3.2.8 of the work plan for UB). As a substitute the focus of the activities was put on the refinement and validation of the ASI algorithm, as described in Section 3.

### 3 Set up of other software (3.2.3)

In order to accurately calculate the clear-sky surface temperature, which is required to estimate the thickness of thin ice via the heat-flux method (see Section 10) the software package CASPR developed by Key (2002) has been obtained and installed. The CASPR software allows to calculating the surface temperature on the basis of calibrated data of the Advance Very High Resolution Radiometer (AVHRR), channels 4 and 5 (10.3-11.3 $\mu\text{m}$  and 11.5-12.5 $\mu\text{m}$ ) (Key et al, 1997). The software was implemented into IDL on a LINUX-Workstation and was used to derive the surface temperature from AVHRR data acquired over the region WRS for the period April to October 2002 and May to September 1999. Examples of the derived surface temperature are given in Section 10.

In order to derive the thin-ice thickness with the heat-flux method (see Section 10) and the net surface heat flux to obtain the ice production as related to the polynyas (see Sections 6 and 9), the 6-hourly analysis of the main meteorological parameters (2m air temperature and humidity, surface air pressure, 10 m u- and v-component of the wind speed) of the Re-Analysis project ERA40 of the European Centre for Medium Range Weather Forecast (ECMWF) are used (Kållberg et al. 2004). This data is available at the Institute of Oceanography, Hamburg, via collaboration with the German Climate Research Centre (DKRZ). In order to read and transform this data into a user-friendly format that can be further used by other software like IDL or Matlab, the PINGO package (<http://www.mad.zmaw.de/Pingo/pingohome.html>) has been obtained, installed, and used to read and transform ERA40 data of the period 01/1992 to 08/2002 for further analysis and application.

As substitute to the missing PSSM algorithm adapted for its application to AMSR-E data because of the problems with the geo-location, the ASI algorithm, which is based on the 89 GHz data of the AMSR-E (Kaleschke et al., 2001; Spreen et al., 2008), has been applied to all AMSR-E data available. Time series of the obtained ice concentrations are available at the Institute of Environmental Physics, Bremen, and the Institute of Oceanography, Hamburg, via the webpage <http://www.seaice.de>. ASI/AMSR-E ice concentrations have been combined with the PSSM/SSMI polynya data. Both data types have a similar horizontal resolution, and the combination has been used to derived a realistic estimates for the ice production for all Antarctic polynyas, see Section 9. In order to better assess the reliability of the used ASI/AMSR-E sea ice concentrations, comprehensive validation studies have been performed (see Section 5).

### 4 Acquire and project evaluation and other data (3.2.4)

About 340 NOAA (14, 15, 16, and 17) AVHRR images have been acquired for modification and evaluation of the PSSM, the improvement of the land mask, and the calculation of the clear-sky surface temperature from the NSIDC Satellite Active Archive (SAA). The data is obtained in LAC format (Local Area Coverage with about 1 km spatial resolution). The data is processed and projected into the same grid as is used for the SSM/I data – with grid-cell sizes of 5 km x 5 km (for an overview, see Figure 7) and 1 km x 1 km for specifically selected areas (see Figure 8) using IDL and FORTRAN routines.

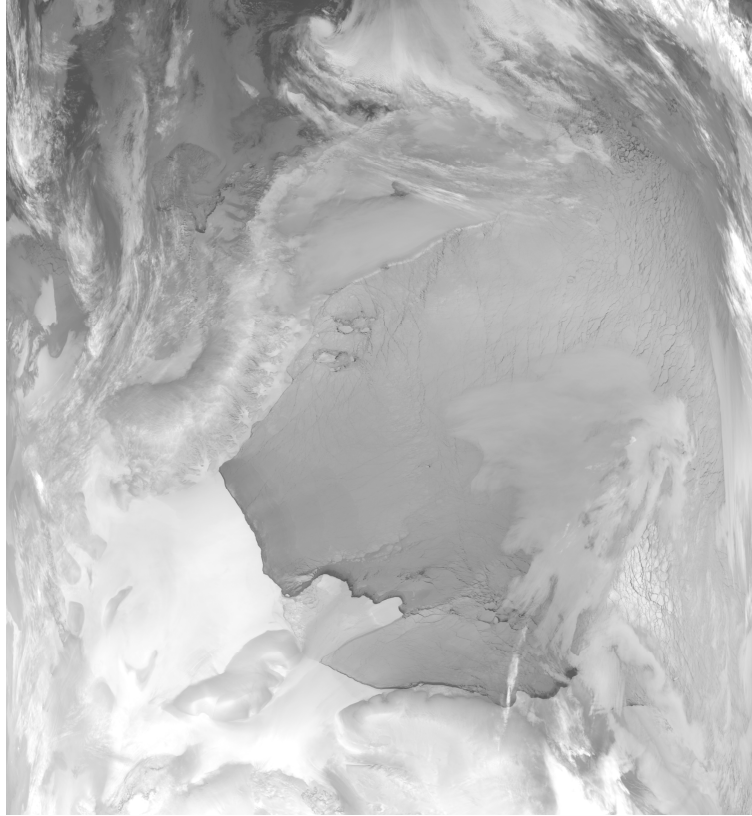


**Figure 7:** NOAA-16 AVHRR image of channel 4 of the Weddell Sea of October 2, 2002, 19:19 UTC (LAC, not projected). Gray-levels are chosen to show the full range of temperatures (white = low, black = high temperatures).

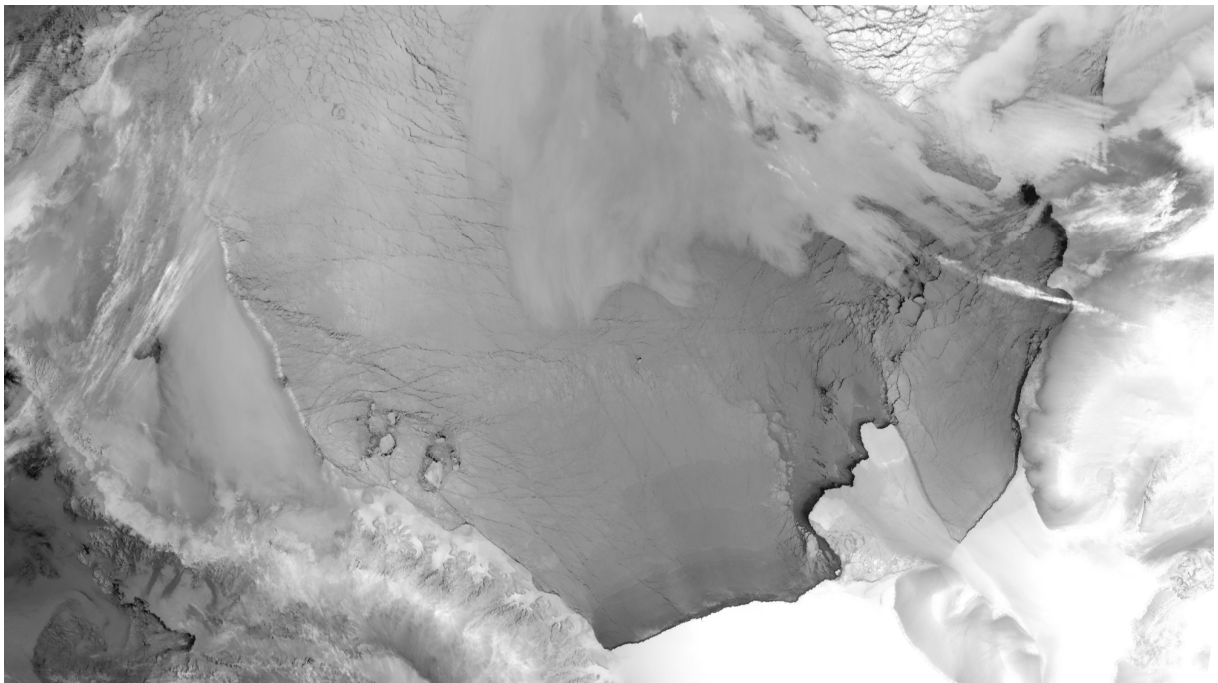


**Figure 8:** Sub-region of the image shown in Figure 7 projected into the fine-mesh version (1km x 1km spatial resolution) of the NSIDC polar-stereographic grid for the Central Weddell Sea (see Figure 6). Gray levels are chosen to achieve best discrimination of relevant features with black: 271K, and white: < 235K.

As already indicated in Section 3, data of the Re-analysis ERA40 of the ECMWF (6-hourly analysis of 2m air temperature and humidity, surface air pressure, 10m wind speed) has been acquired. This data has been transformed to a different, user-friendly format using the PINGO-package, and data covering the Southern Ocean / Antarctica has been selected for the period 01/1992 until 08/2002 (the ERA40 time series stops here). Subsequently the data has been interpolated to the same fine-meshed version of the NSIDC grid that is used for the PSSM, i.e. with 5 km x 5 km grid cell size.

Difficulties arising during the calculation of appropriate net surface heat fluxes on the basis of the ERA40 data and hints from the literature (e.g. van Woert, 1999) led to the acquisition of meteorological data as obtained from the net of Automatic Weather Stations (AWS) in the Antarctic. These AWS stations measure the air temperature, air pressure and wind speed – typically at heights between 2 and 4 meters above the ground. The two main sources for the AWS data taken are the Australian Antarctic Division (see e.g. <http://aws.acecrc.org.au/awswebsite/background.html>) and the Antarctic Meteorological Research Center (AMRC) at the Space Science and Engineering Centre (SSEC) in Wisconsin (see <http://ice.ssec.wisc.edu/aws.html>). Where available data of the full period, i.e. 1992-2001 has been obtained for the months May through September from stations marked on the map given in Figure 9.

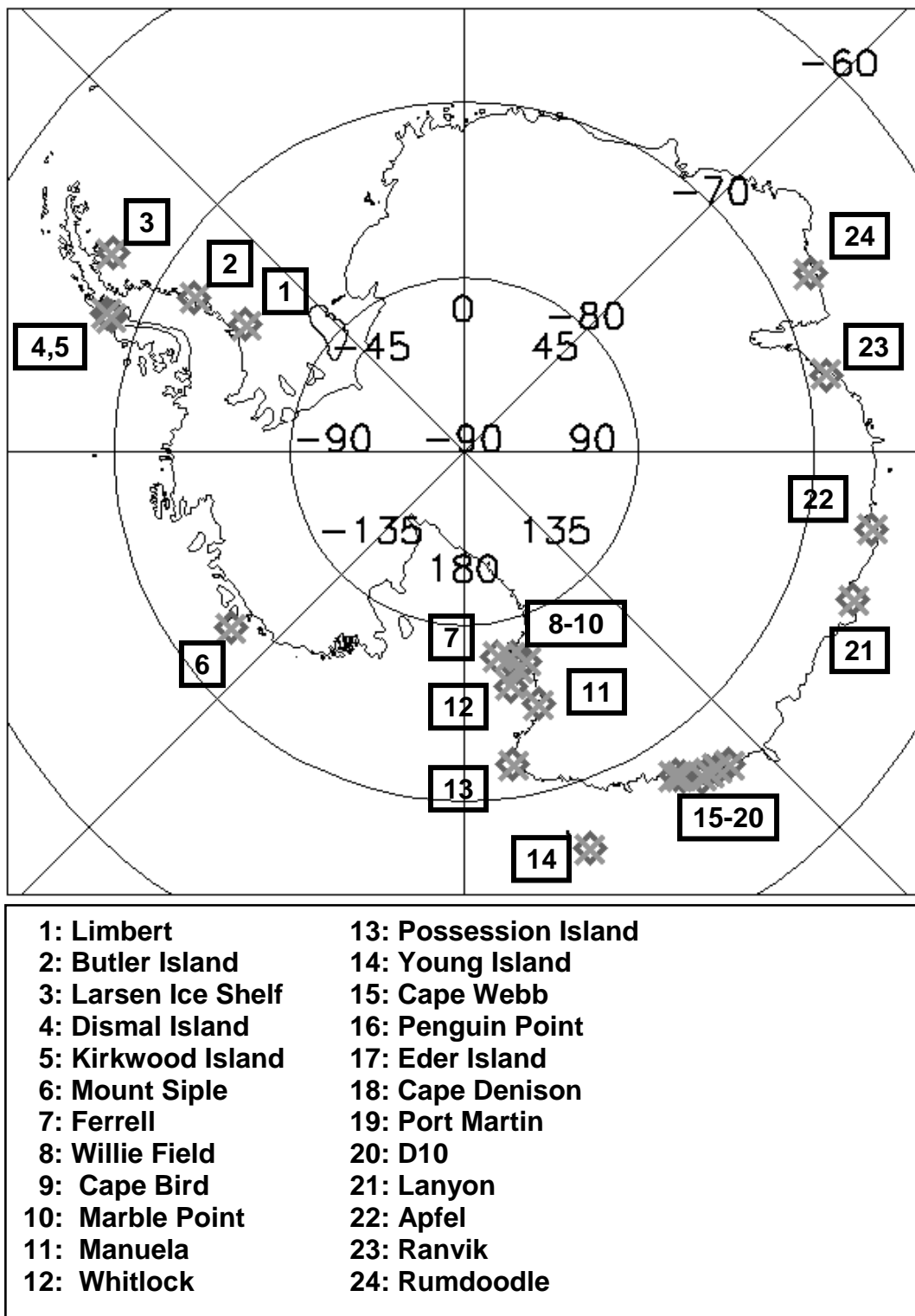


**Figure 9:** Map of Antarctica and the location of the AWS data of which is used for comparison with ERA40 data.

## 5 Apply & evaluate PSSM on test periods and regions (3.2.5)

### 5.1. Evaluation of the PSSM based on SSM/I data

For testing and evaluation the modified PSSM (as a synthesis of PSSM and IED) has been applied for data acquired during November 2002 and March 2003 in the Kara Sea and September/October 2002 in the Southern Ocean (all regions, see Figure 2). Thin ice and open water area were calculated from SSM/I data of DMSP-f13 and -f15. Figure 10 shows an example of maps of the polarization ratio at 37 and 85 GHz, the resulting polynya distribution map derived with the PSSM, and the corresponding COMISO-Bootstrap ice concentration for the Kara Sea.

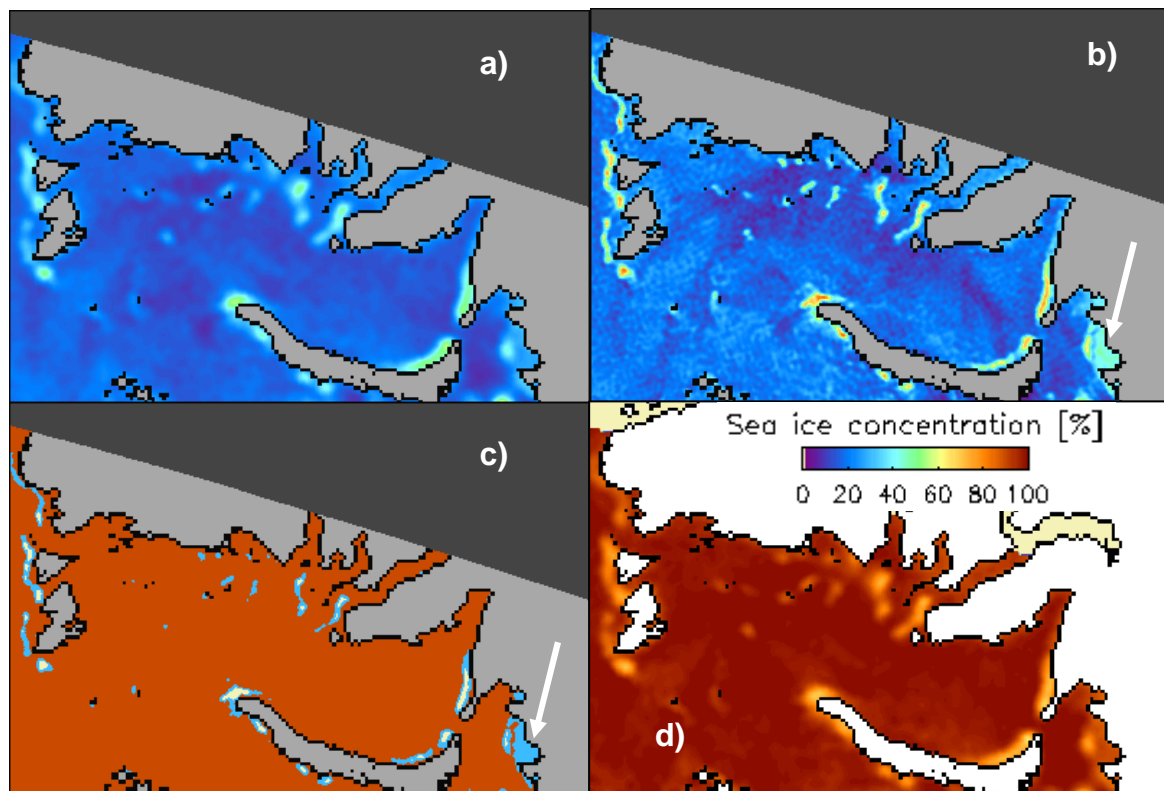


**Figure 10:** Sample set of  $P$  at 37 GHz (a), at 85 GHz (b), the resulting PSSM map (c) and the corresponding COMISO-Bootstrap ice concentration (d) for the Kara Sea, March 11, 2003, 8 UTC (Siberian coast at the top, Novaja Semlja at the bottom, Severna Semlja to the left). Values in (a) and (b) range from dark blue/violet = 0.0 to orange/red = 0.18 (a) and = 0.12 (b). In (c) orange/red denotes thick/consolidated ice, blue thin/loose ice, and white/pale yellow open water. Land appears gray (a to c) or white (d), coasts are black, missing data are dark gray (a to c) or white/pale yellow (d). The white arrows indicate a fast ice area, which apparently can also be a problem in the Kara Sea. However, this fast ice patch is located outside the Kara Sea in the Petchora Sea and therefore does not influence the polynya area retrieval in the Kara Sea itself. Errors due to fast ice coverage in the Kara Sea have been found to be negligible. The same applies to the river (fresh water) ice, which is flagged in a post-processing step before the polynya area time series is calculated.

See Figure 3 and 4 for examples of the Southern Ocean. Maps of the polynya distribution derived with the PSSM but also of the polarization ratios are compared with about 80 AVHRR images for March 2003 and about 25 AVHRR images for November 2002.

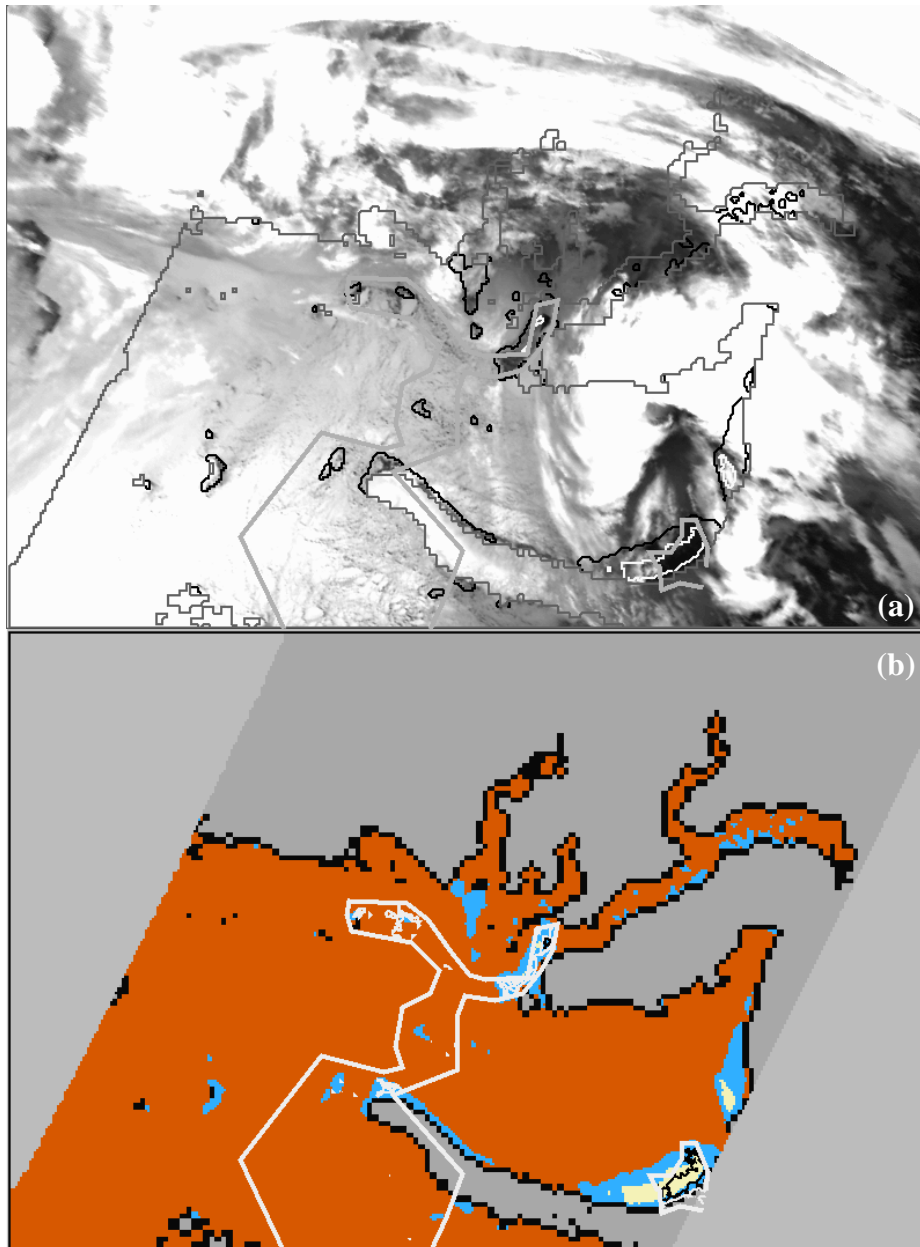


**Figure 11:** (a) AVHRR image, channel 4, of the Kara Sea for March 14, 2003, 11 UTC, superposed by PSSM isolines for the transition thick – thin ice (black) and thin ice – open water (white). The thick gray line gives the area selected as primarily being cloud free (see (b), thick white line); (b) PSSM map of surface types superposed with isolines of surface-temperature estimates from channel 4 at  $-1.8^{\circ}\text{C}$  (thin black) and  $-9^{\circ}\text{C}$  (thin white). Orange/red denotes thick/consolidated ice, blue thin ice, and white/pale yellow open water. Land appears dark gray, coasts are black, missing data are medium gray.

Maps of AVHRR IR-temperature are superposed with isolines denoting the transition thick ice – thin ice and thin ice – open water (Figure 11 a). Maps showing the thick ice, thin ice, and open water distribution are superposed by isolines at  $-1.8^{\circ}\text{C}$  (open water – thin ice transition) and  $-9^{\circ}\text{C}$  (approximate thin ice – thick ice transition) (Figure 11 b). For the latter temperature values of  $-6^{\circ}\text{C}$  and  $-12^{\circ}\text{C}$  have also been tested but are not used, because these values led to unrealistic distributions of thin ice. This comparison is only possible for cloud-free areas, which have been delineated manually in every used AVHRR image. The comparison is merely based on AVHRR data acquired at channel 4; if daylight permits

AVHRR data acquired at channel 1 are used as well. For the latter a sun-incidence angle correction has been applied in order to optimize the gray-level distribution and to increase the usable area of a particular image. The outcome of these comparisons helped not just to evaluate the final PSSM map but also to tune the tie points mentioned in section 2 to achieve optimum agreement between the polynya area obtained with the PSSM and the polynya area as seen in AVHRR imagery.

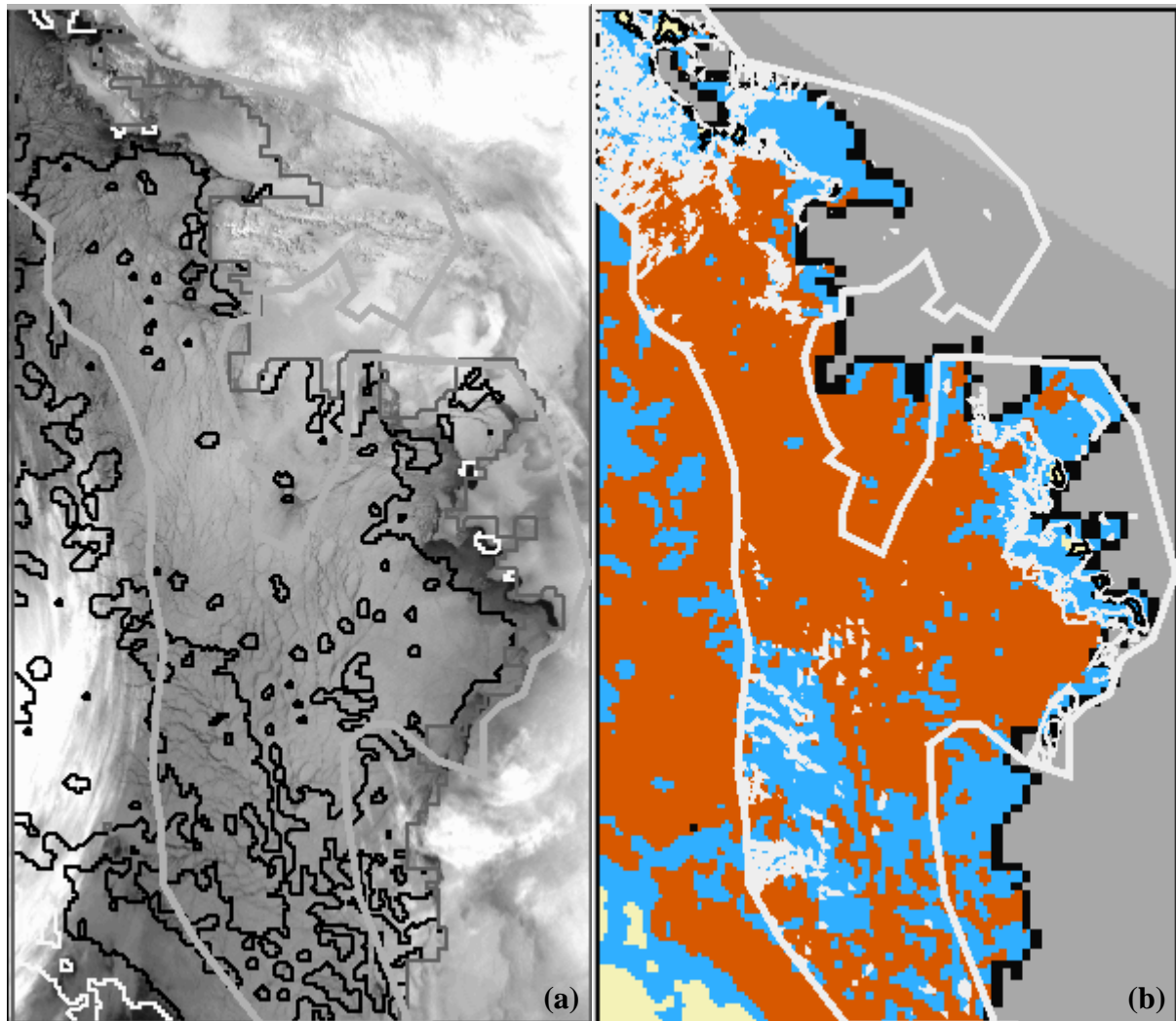


**Figure 12:** Example of the evaluation for region EBS for Oct. 7, 2002; a) AVHRR image acquired with channel 4, superposed with isolines of the transition open water – thin ice (white lines) and thin ice – thick ice (black lines) as found by the PSSM. The thick grey lines encloses the cloud-free area (see thick white line in b); b) PSSM polynya distribution map superposed with isolines of surface-temperature estimates from AVHRR channel 4 at  $-1.8^{\circ}\text{C}$  (thin black) and  $-9^{\circ}\text{C}$  and  $-12^{\circ}\text{C}$  (thin white). Note that these isolines are only given in the cloud-free area marked by the thick white line. Land and coastlines are marked grey and black respectively. For color coding of the PSSM map see Figure 4. None of the other masks are shown here in order to get the full picture.

The Figures 12 and 13 show one example each of the comparison between PSSM polynya distribution maps and AVHRR imagery for the regions EBS and EIS. This comparison / evaluation had been done similar to what has been described for the Kara Sea. In total about 220 AVHRR images are used to tune the PSSM and to separately evaluate the results obtained for all nine regions (see Figure 2). Figure 12 b) reveals about eight open water areas seven of

which are found with the PSSM (see white isolines in the cloud-free area in Figure 12 a). Figure 13 b) reveals also about eight open water areas eight of which are found by the PSSM (see white isolines in the cloud-free area in Figure 13 a).

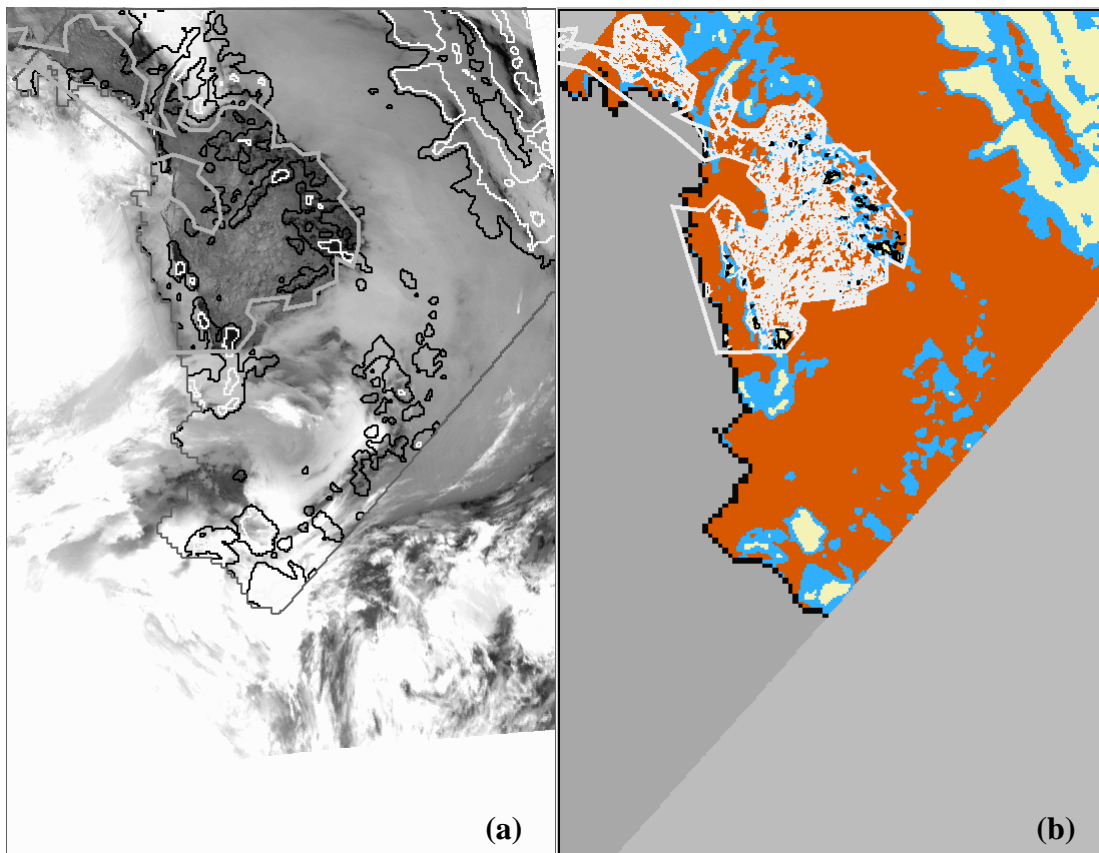


**Figure 13:** As Figure 12 but for the region EIS for October 21, 2002. Note that the size of the shown image is just half the original size.

## 5.2 Validation of ASI/AMSR-E ice concentrations

As is mentioned in Section 3, problems with the geo-location of AMSR-E data, delayed the adaptation of the PSSM to AMSR-E data. Instead more emphasis was put on the ASI algorithm.

The ASI algorithm has been extensively validated in a number of studies with four different types of independent validation data:

- Comparison with ship-borne observations from R/V Polarstern in the Arctic (see Spreen et al., 2008; Heygster et al., 2008).
- Validation with EMT+/Landsat-7 data in the Bering Sea and Bering Strait (see Wiebe, 2007; Heygster et al., 2008).
- Comparison with SAR-derived ice concentrations from the Arctic (see Spreen et al., 2008; Heygster et al., 2008).
- Comparison with NASA Team-2 and Bootstrap Algorithms (NT2 and BT) from the Arctic and the Antarctic (Spreen et al., 2008; Heygster et al., 2008).

The comparisons of the ASI, NT2 and BT results with ship observations from cruises in three different years give a rather consistent picture: with one exception (NT2 during ARK XXII), the biases of all three algorithms coincide within 3 % bias and 2% RMS error.

Consistently over all four analyzed Landsat scenes, the ASI algorithm detects first-year ice

with an accuracy, that is very similar to that achieved with the NT2 algorithm (bias below 1%, RMS errors 1 to 4 %). For young and even more for new ice (which cover much less area) the bias and RMS error increase, for new ice up to 26%. Note, however, that the comparison of ASI ice concentration data with the ice concentration obtained independently from Landsat and SAR scenes yields different results; obviously this data (Landsat and SAR) considered as ground truth detect different ice types differently. Areas that are identified as new ice by the optical sensor have higher ice concentrations compared to those indicated by the ASI algorithm. So, the ASI algorithm tends to under-estimate the ice concentration when new ice is present. On average, the ASI ice concentrations range between those from Landsat and SAR. Both the bias intervals (-2.9 % to +2.6 %) and the RMS errors are slightly higher than those of the NT2 algorithm, applied to the same scenes.

In order to overcome the limitations of regionally and seasonally limited case studies, the differences between the ASI and the NT2 and BT results, respectively, have been determined independently for both hemispheres and over the years 2002 to 2006. The biases of the four cases do not exceed 2%, the RMS error ranges between 7 and 11% ice concentration (Sprenn et al., 2008). At first glance, these RMS errors may appear relatively high. However, none of the three involved ice concentration data sets can be regarded as 'ground' truth. Rather, they all three carry their own errors as the different choice of channels in use determines the sensitivity of the algorithms to direct and indirect weather influences, ice thickness and ice surface properties.

According to Parkinson and Comiso (2008) the mean monthly ice concentration obtained with the NT2 and the BT from AMSR-E data for May and August, 2003 to 2006, drop down to values of 80 % to 85 % in those areas around Antarctica, which are sites of recurring polynyas, i.e. the Ross Sea, around the Mertz Glacier polynya and along the East Antarctic coast. The differences between these two algorithms in these areas are less than five percent. According to Sprenn et al. (2008) ice concentrations averaged over the period June 19, 2002, to August 31, 2006, tend to be lower in these areas by up to 8 % when using the ASI algorithm instead of the NT2 or the BT. Note, that these areas of reduced ice concentration are also smaller in size compared to the other two algorithms. This is both caused by the enhanced spatial resolution achieved with the ASI algorithm; with which the ice concentration ice obtained with spatial resolution of the order of 5 km x 5 km, instead of 12.5 km x 12.5 km as is typical for the other two algorithms. A similar conclusion was drawn by Kern (2004) who compared ice concentrations, which were derived with 85 GHz SSM/I data on a grid with 12.5 km grid cell size, with the NASA-Team algorithm ice concentration available with 25 km grid cell size. Therefore the ASI algorithm has been chosen to use it in combination with the PSSM applied to SSM/I data.

## 6 Perform analysis of ice production (3.2.6)

Ice and salt production as associated with the observed polynyas is calculated as follows:

- Take ECMWF ERA40 data (air temperature and humidity, wind speed, surface pressure) and interpolate this data onto the fine-mesh (5 km grid cell size) version of the NSIDC-grid used to get the polynya distribution with the PSSM (see Section 4).
- Restrict the further calculation and analysis to the months April (May) to September to minimize the influence of solar radiation, which in fact is neglected here.
- The net surface heat flux then comprises the net long-wave heat flux and the turbulent fluxes of sensible and latent heat (see e.g. Van Woert, 1999). The following formulas are used to calculate the net surface heat flux. At first the net surface heat flux  $F_t$  is given by:

$$F_t = F_s + F_l + F_{up} + F_{down}$$

$F_s$ ,  $F_l$ ,  $F_{up}$ , and  $F_{down}$  are the sensible, latent, long-wave emitted, and long-wave downwelling fluxes, respectively. The sensible and latent heat fluxes are calculated using common bulk formulae:

$$F_s = \rho_{air} \cdot c_p \cdot C_s \cdot u \cdot (T_{air} - T_{surface})$$

$$F_l = \rho_{air} \cdot L \cdot C_s \cdot u \cdot (q - q_{surface})$$

In these two equations  $\rho_{air} = 1.3 \text{ kg / m}^3$  is the density of cold air,  $c_p = 1004 \text{ J / kgK}$  is the specific heat of dry air,  $C_s = 0.0018$  is the bulk transfer coefficient for heat / moisture (at a height of 2 m),  $u$  is the wind speed at a height of 2 m,  $L = 2.5 \times 10^6 \text{ J/kg}$  is the latent heat of evaporation,  $T_{air}$  is the air temperature at a height of 2 m,  $T_{surface}$  is the surface temperature and set to the temperature of freezing sea water:  $-1.8^\circ\text{C}$ ,  $q$  is the specific humidity at a height of 2 m, and  $q_{surface}$  is the specific humidity at the surface. The value used for the bulk heat transfer coefficient is 0.0018. This differs from values reported in the literature and used for similar purposes. For example, Yu and Lindsay (2003) and Drucker et al. (2003) used a value of 0.003, which was deduced from in-situ measurements over narrow leads (Lindsay and Rothrock, 1994). These values are, however, valid for a height above ground of 10 m and a temperature difference between the surface and the air of at least 10 K. Andreas et al. (1979) and Andreas and Murphy (1986) defined the bulk transfer coefficient over Arctic leads to be between 0.0021 and 0.0025 at a height of 2 m above sea level, but only 0.0013 at a 10 m height. Over open water they defined  $C_s$  as being 0.001. Finally, by carrying out air-borne measurements Walter et al. (2006) found values for  $C_s$  of about 0.0012 for a mixture of thick ice and leads valid for a height above ground of 10 m.

So the value of  $C_s$  to be used in bulk formulae to calculate the turbulent sensible and latent heat fluxes depends on the height above ground for which this calculation is carried out and on the temperature / humidity difference between the surface and the air. In this study the calculation are carried out for a height of 2 m above the ground so values like 0.003 and/or 0.0021 to 0.0025 seem to be appropriate – however only for small leads / polynyas and a large temperature difference. In order to account for the fact, that most of the polynyas considered in this study are quite large, a value between the open water value to those given above is chosen: 0.0018.

The wind speed in the ERA40 data is given for a height of 10 m above the ground. Using the logarithmic wind profile equation the wind speed at 2 m height above ground can be approximated as follows  $u_{2m} = u_{10m} / 5^{0.3}$ . The specific humidity is calculated via computation of the partial water vapour pressure from the dew-point temperature using the Clausius-Clapeyron formula using coefficients valid for saturation with respect to ice. For  $q_{surface}$  it is assumed, that the relative humidity directly at the surface is 100 % so that the partial water vapour pressure at the surface equals the saturation water vapour pressure at a surface of  $T_{surface} = -1.8^\circ\text{C}$  with saturation with respect to ice.

Finally for the net long-wave heat flux  $F_{up-down}$  the parameterization of Berliand and Berliand (1952) is used:

$$F_{up-down} = \epsilon \sigma T^4 (0.39 - 0.05 \sqrt{e_0}) (1 - 0.9 \cdot C) + 4 \epsilon \sigma T^3 (T_{surface} - T).$$

Here  $\varepsilon = 0.98$  is the long-wave emissivity,  $\sigma = 5.67 \times 10^{-8} \text{ W/m}^2$  is the Stefan-Boltzmann constant,  $T$  is the air temperature at 2 m height,  $C$  is the cloud coverage, and  $e_0$  is the saturation water vapor pressure at the surface.

Having the net total surface heat flux the ice production can be calculated using:

$$P_{\text{ice}} = F_t / \rho_{\text{ice}} \cdot L_h$$

where the ice production  $P_{\text{ice}}$  is the total net heat flux  $F_t$  divided by the density of the ice (frazil ice)  $\rho_{\text{ice}} = 950 \text{ kg/m}^3$  and the latent heat of fusion  $L_h = 334 \text{ J / kg}$ .

## 7 Comparison with models (3.2.7)

### 7.1 Kara Sea

Maps of the polynya distribution as obtained with the PSSM for the Kara Sea for 1999-2004 are compared to maps of the ice compactness (ice concentration) derived with the HAMSOM (HAMBurg Shelf Ocean Model) model. For the period February 1-16, 2001, a direct comparison between PSSM maps of the polynya distribution, maps of the COMISO Bootstrap ice concentration and the ice concentration as modeled with HAMSOM has been carried out.

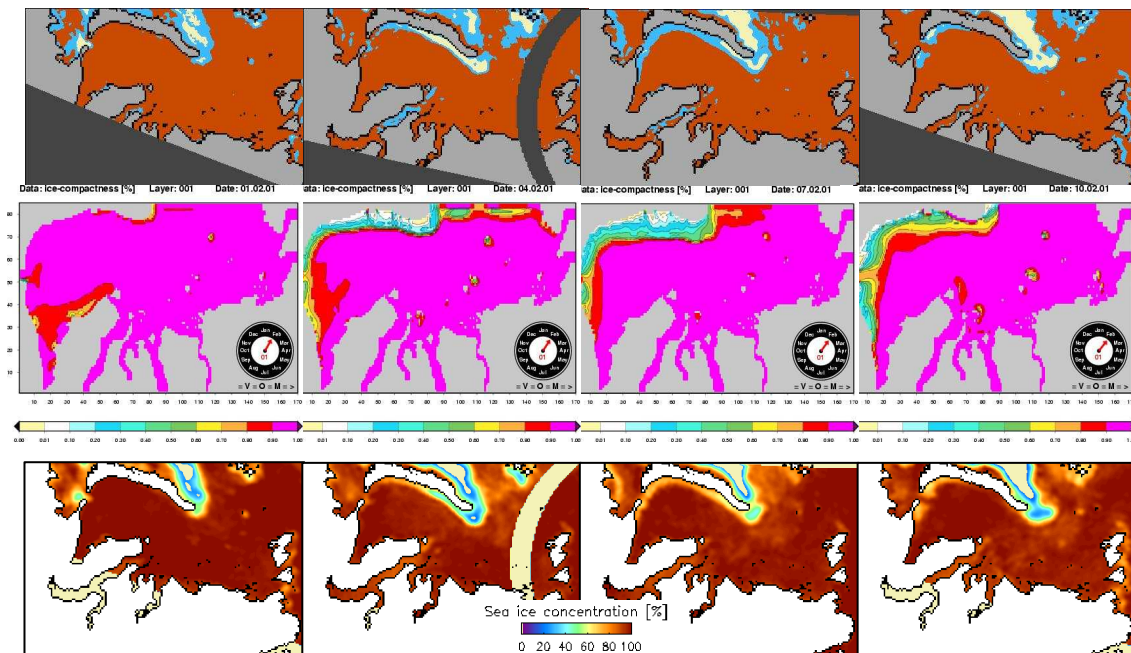


**Figure 14:** Top row: PSSM map showing the extent of thick/consolidated ice (red/brown), thin/loose ice (blue), and open water (white/pale yellow) for the Kara Sea (Siberian coast at bottom, Novaja Semlja at top, Severna Semlja right) for February 1, 4, 7, and 10, 2001, going from left to right; middle row: HAMSOM ice concentration; bottom row: COMISO-Bootstrap ice concentration.

A sample set of this comparison is shown in Figure 14. This Figure demonstrates basically three things:

- Locations of thin/loose ice and open water in the PSSM maps agree with the HAMSOM ice concentration.
- During this event ice is pushed away from the eastern coast of Novaja Semlja over a long distance permitting a large polynya to develop (February 4) which gradually

closes (more thin/loose ice instead of open water in PSSM map and less steep ice-concentration gradient in HAMSOM map, February 7 compared to February 4) and, which shifts towards the southwest (February 10).

- c) The COMISO-Bootstrap algorithm captures this event by yielding lower ice concentrations in the polynya area. However, open water is usually missed.

The latter fact is evident more clearly from Figure 15, showing thin ice and open water area together with the average COMISO-Bootstrap ice concentration. The average ice concentration for the thin ice area takes values of about 75 %, the one for the open water area amounts about 55 %, values which both cannot reflect the conditions met in reality.

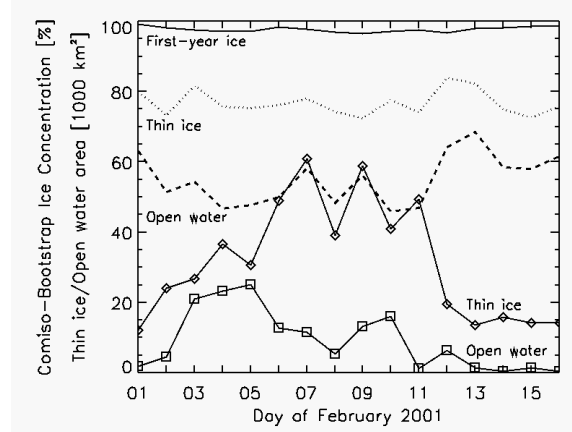


**Figure 15:** Thin/loose ice (diamonds) and open water (squares) extent in the Kara Sea for February 1-16, 2001, as obtained with the PSSM in comparison to the average COMISO-Bootstrap ice concentration for the thick/consolidated (first-year) ice area (solid line), the thin/loose ice area (dotted line), and the open water area (dashed line).

The polynya area time series of the Kara Sea, which will be shown in Figure 19, has been compared with the compactness of the ice cover in the Kara Sea as obtained from sea-ice concentration maps derived with the COMISO-Bootstrap and/or NASA-Team algorithm (see Kern et al., 2006) and the export of sea ice out of the Kara Sea towards the north as obtained with HAMSOM. The main result of this comparison is that winters with a high (low) sea-ice export out of the Kara Sea coincide with a reduced (increased) compactness of the ice cover and a higher (lower) mean total polynya area (Kern et al., 2005). Therefore, in this case the output of HAMSOM in terms of sea-ice export could be used to get a first guess of the total polynya area / polynya activity during the considered winter.

## 7.2. Southern Ocean

A two dimensional, steady state polynya flux model (Biggs et al., 2000) has been applied to the polynya regions marked by the red boxes in Figures 17 and 18 in regions EIS and WRS, respectively. The model is based on the following equation describing the motion of the polynya edge  $C(X,0)$  in time. As time tends to infinity in the solution of this equation, the steady state polynya edge is traced out. The balance is found when the ice forming within the polynya reaches the pack ice at the polynya edge and piles up against it. Figure 16 shows the

$$C_t + \frac{d\mathbf{X}}{dt} \cdot \nabla C = 0$$

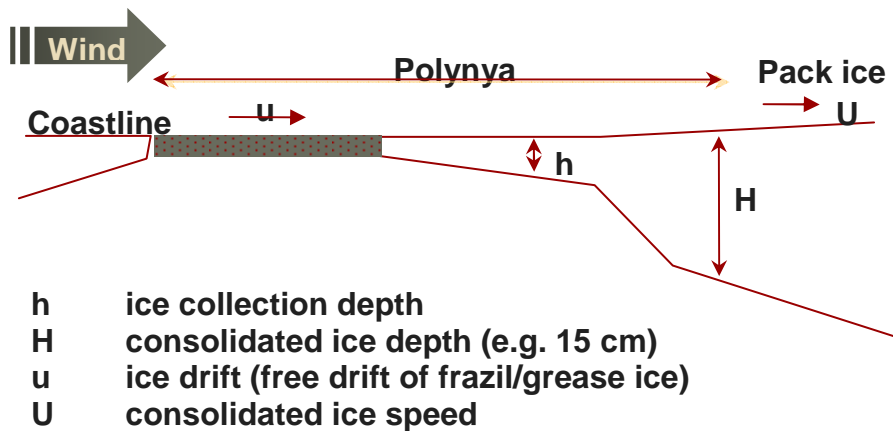


**Figure 16:** Scheme of a polynya as realized in the polynya flux model.

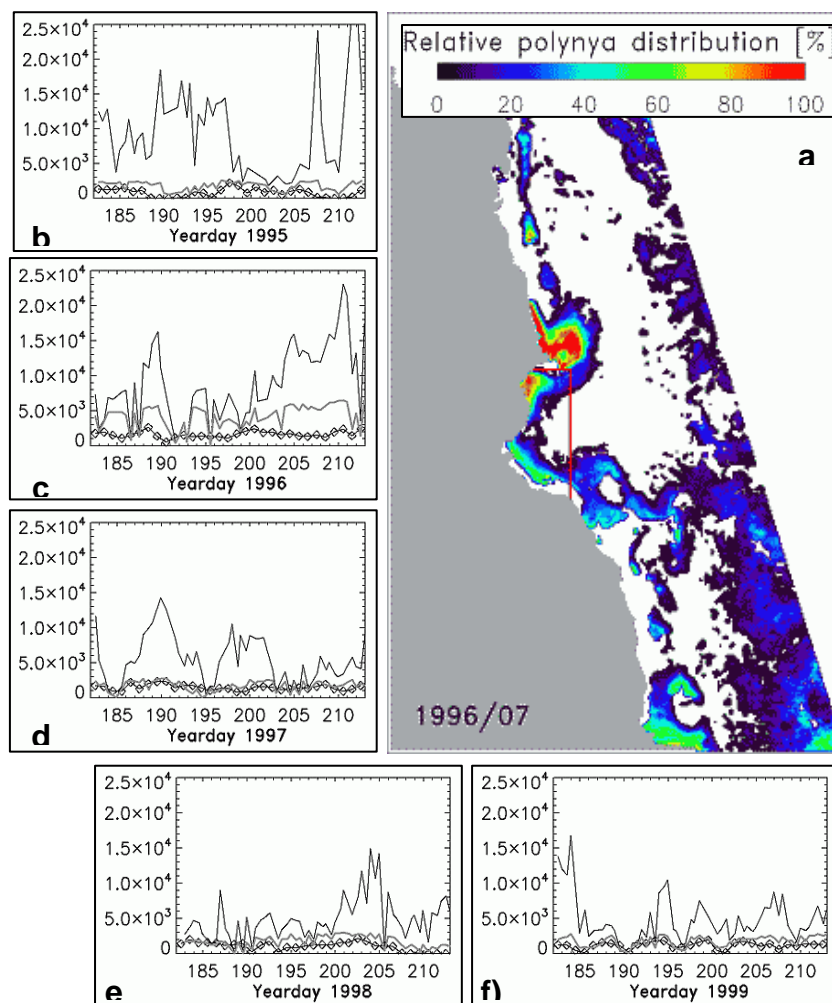


**Figure 17:** Map: relative frequency of occurrence of a polynya in each 5km x 5 km grid cell of the region EIS for July 1996. A value of 50 % (transition from light blue to green) indicates that on 50 % of the included PSSM-maps of the polynya distribution in July a polynya has been observed. Graphs b) to f): Comparison between modeled (diamonds) and PSSM-based total polynya area for the Prydz-Bay / Amery Ice Shelf area (see red line in map) for July of the years 1995-1999. The graphs show the total polynya area and that polynya area, which lies inside the line given by a 50 % probability for the occurrence of a polynya in July of the respective year.

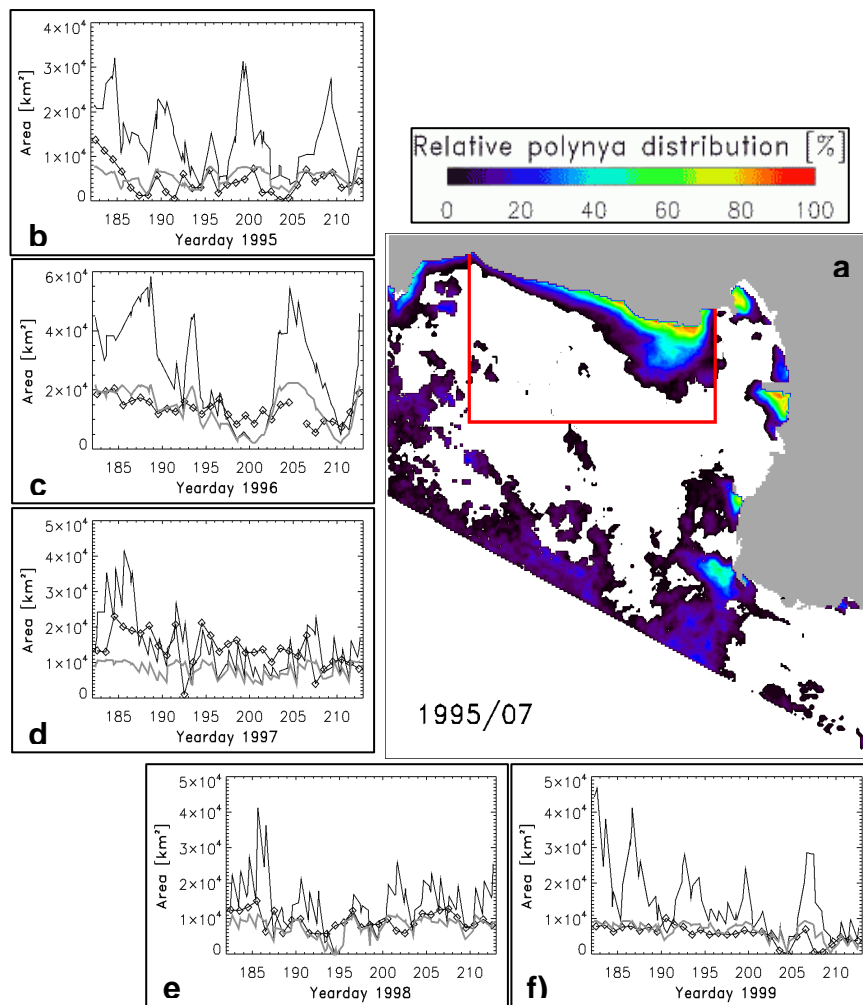


**Figure 18:** Same as Figure 17 but for the region WRS and the Ross Ice Shelf polynya. The map shown in a) is the relative polynya distribution for July 1995. Note the different scale of the y-axis.

scheme of a model polynya. Input for the model is wind speed, air temperature, dew point data taken from 6-hourly analysis of the global operational ECMWF weather forecast model. Net surface heat fluxes and the ice production are calculated by using bulk formulae given by Van Woert (1999).

Figures 17 and 18 give a comparison between the polynya area as obtained with this steady state polynya flux model (SSPFM) on the one hand (diamonds in images b) to f)), and the polynya area as obtained with the PSSM on the other hand (solid lines without symbols). The comparison has been done for the month of July for 1995-1999 and reveals the following results:

- The polynya area obtained with the PSSM is much more variable than the one based on the SSPFM
- The polynya area based on the PSSM is much larger than the one obtained with the SSPFM. The latter takes values between 0 and 2000 km<sup>2</sup> for the Prydz-Bay polynya and between 0 and 23 000 km<sup>2</sup> for the Ross-Ice Shelf polynya region. The over-estimation of the polynya area by the PSSM relative to the one obtained with the SSPFM is larger for the Prydz-Bay polynya.

This discrepancy could be explained based on the following facts. First, the Prydz-Bay polynya area is much more subject to catabatic winds blowing down the Antarctic continent. These winds are a local phenomenon and are steered by the topography. The model data used

to force the SSPFM are taken from the ECMWF global weather forecasting model with a grid resolution of  $1.125^\circ \times 1.125^\circ$ . At such a spatial resolution the steep topography, which is typical for almost the entire Antarctic coastline, is certainly smoothed. This results in less pronounced catabatic winds, and thus in a potentially smaller wind speed than would have been observed in reality (see Section 9). According to a detailed investigation a doubling of the wind speed yields almost a doubling of the polynya width at constant temperature (Flocco, 2007). Note, that when limiting the polynya area by the 50 % probability iso-line (see map a) in Figures 17 and 18) for the occurrence of a polynya in July of the respective months, the agreement between the SSPFM-based and the PSSM-based polynya area increases substantially (see thick grey lines in images b) to f) in Figures 17 and 18).

Finally it has to be stressed that the PSSM-based polynya area is totally independent of the SSPFM result, i.e. cases in which the model (SSPFM) data do not (yet) favor the development of a polynya at all might coincide with a well developed polynya as observed with the PSSM and vice versa. Additionally it has to be noted that while in the PSSM-based data set the transition between thin and thick ice, i.e. the edge of the polynya, is at approximately 10 cm ice thickness (see Section 10) this is more difficult to give a fixed thickness value describing the edge of the polynya in the SSPFM data set (see Figure 16). Thickness values at the polynya edge depend on the wind speed and the pre-defined value of H (Figure 16) and may take values between 5 and 25 cm.